

CHEMISTRY IN DENSE PHOTON-DOMINATED REGIONS

A. STERNBERG

School of Physics and Astronomy, Tel Aviv University, Ramat Aviv 69978, Israel

AND

A. DALGARNO

Harvard-Smithsonian Center for Astrophysics, 60 Garden Street, Cambridge, MA 02138

Received 1994 March 17; accepted 1994 August 10

ABSTRACT

We present a detailed chemical model of a photon-dominated region produced in a dense molecular cloud exposed to an intense far-ultraviolet radiation field. We use it to illustrate the gas-phase processes that lead to the production of atomic and molecular species in the several distinct zones that occur in the cloud. We identify molecular diagnostics of photon-dominated chemistry in dense molecular clouds.

Subject headings: galaxies: ISM — ISM: molecules — molecular processes

1. INTRODUCTION

Photon-dominated regions (PDRs) form in neutral hydrogen clouds which are exposed to far-ultraviolet (FUV) radiation fields (6–13.6 eV) from external sources (de Jong, Dalgarno, & Boland 1980; Tielens & Hollenbach 1985; Sternberg & Dalgarno 1989). PDRs are ubiquitous in the interstellar medium and are present at the edges of H II regions (Stacey et al. 1993; van der Werf et al. 1993; Zhou et al. 1993; Hogerheijde, Jansen & van Dishoeck; van der Werf et al. 1995), planetary nebulae (Graham et al. 1993; Latter, Walker, & Maloney 1993), and reflection nebulae (Fuente et al. 1993; Jansen, van Dishoeck, & Black 1994), inside clumpy molecular clouds in star-forming regions (Stutzki et al. 1988; Lane et al. 1990; Howe et al. 1991; Meixner et al. 1992), the Galactic center (Genzel, Hollenbach, & Townes 1994), and starburst galaxy nuclei (Stacey et al. 1991; Henkel, Baan, & Mauersberger 1991; Krabbe, Sternberg, & Genzel 1994; Sternberg et al. 1994), and probably in the narrow-line regions of active galactic nuclei (Planesas, Scoville, & Myers 1991; Rotaciuc et al. 1991; Jackson et al. 1993; Blietz et al. 1994; Tacconi et al. 1994).

The physical and chemical properties of PDRs are controlled by the incident FUV photons which both heat the gas and drive the cloud chemistry in sequences initiated by photoionization and photodissociation. The gas temperatures in PDRs range from ~ 20 to $\gtrsim 1000$ K, and they are often detectable sources of infrared and millimeter atomic and molecular line emission. In recent years it has become possible to study individual PDRs in great detail using the multiwavelength techniques of ground-based and air-borne infrared imaging spectroscopy, heterodyne submillimeter spectroscopy, and millimeter wave interferometry (Harris et al. 1987; Jaffe & Howe 1989; Genzel, Harris, & Stutzki 1989; Hollenbach 1990; Poglitsch et al. 1991; Genzel 1992; Phillips 1992; Krabbe et al. 1993; Sargent & Welch 1993; Tielens et al. 1993). These observational studies will continue throughout the next decade. A major development will be the observation of PDRs from space using mid- and far-infrared spectrometers on board

the *Infrared Space Observatory (ISO)* (Encrenaz & Kessler 1992).

Theoretical models of photon-dominated regions have been constructed and developed by several research groups (e.g., Tielens & Hollenbach 1985; van Dishoeck & Black 1988; Sternberg & Dalgarno 1989; Le Bourlot et al. 1993; Köster et al. 1994) and have been used successfully to interpret a wide variety of multiwavelength Galactic and extragalactic emission-line data. Comprehensive chemical models of low-density diffuse and translucent clouds have been presented by van Dishoeck & Black (1986, 1989). However, they did not investigate molecule formation in dense clouds which fully absorb the incident FUV radiation. Many models of optically thick PDRs have been presented in the literature (Tielens & Hollenbach 1985; Black & van Dishoeck 1987; Sternberg 1988; Sternberg & Dalgarno 1989; McKee 1989; Wolfire, Hollenbach, & Tielens 1993; Burton, Hollenbach, & Tielens 1990; Wolfire, Tielens, & Hollenbach 1990; Hollenbach, Takahashi, & Tielens 1991; Elmegreen 1993; Le Bourlot et al. 1993; Meixner & Tielens 1993; Köster et al. 1994; Goldshmidt & Sternberg 1995). These authors focused on the FUV absorption properties of such clouds, and on the atomic fine-structure and H₂ and CO line emissions produced in the clouds, and presented limited discussions of the cloud chemistry.

In this paper we present a detailed chemical model of a photon-dominated region produced in a dense molecular cloud exposed to an intense far-ultraviolet radiation field. We use our calculations to illustrate the various gas-phase photochemical processes that lead to the efficient production of atomic and molecular species in dense PDRs.

2. MODEL

The physical and chemical properties of photon-dominated regions depend on several cloud parameters including the (hydrogen) gas density and pressure, the intensity of the incident FUV radiation field, the absorption and scattering properties of the dust grains, the gas-phase elemental abundances, and the clumpiness of the clouds. All of these quantities vary

considerably in the wide range of possible interstellar environments.

Our model consists of a static, plane-parallel, semi-infinite cloud which is exposed, on one side, to an isotropic FUV field. In our calculations we assumed a constant hydrogen particle density $n_T = 10^6 \text{ cm}^{-3}$ throughout the cloud, and adopted an incident FUV field equal to Draine's (1978) fit to the average interstellar FUV field multiplied by an intensity scaling factor $\chi = 2 \times 10^5$.

We used our model to compute the depth-dependent densities of the hydrogen family H, H₂, H⁺, H₂⁺, H₃⁺; the oxygen family O, O⁺, OH, H₂O, OH⁺, H₂O⁺, H₃O⁺, O₂, and O₂⁺; the carbon family, C, C⁺, CH, CH₂, CH₃, CH₄, CH⁺, CH₂⁺, CH₃⁺, CH₄⁺, and CH₅⁺; the sulfur family S, S⁺, SH, H₂S, SH⁺, and H₂S⁺; the nitrogen family N, N⁺, NH, NH₂, NH₃, NH⁺, NH₂⁺, NH₃⁺, NH₄⁺, N₂, and N₂H⁺; the silicon family Si, Si⁺, SiH, and SiH₂⁺; the oxygen intermediates CO, CO⁺, HCO⁺, SO, SO₂, SO⁺, NO, NO⁺, SiO, SiO₂, SiO⁺, and SiOH⁺; and the carbon intermediates CS, CS⁺, HCS, HCS⁺, CN, HCN, CN⁺, HCN⁺, H₂CN⁺, and OCS.

The chemical structure depends on the total gas-phase abundances of the heavy elements. For the volatile elements, carbon, nitrogen, oxygen, and sulfur, we adopted approximately solar abundances equal to, respectively, 3×10^{-4} , 1×10^{-4} , 6×10^{-4} , and 1×10^{-5} relative to hydrogen. We adopted a depleted abundance of 1×10^{-6} for the refractory element silicon. We assumed that the total elemental abundances do not vary with cloud depth.

We computed the atomic and molecular densities by solving equilibrium chemical equations of the form

$$\sum_{jl} k_{ijl}(T)x_jx_l + \sum_j [\Gamma_{ij}(z) + \xi_{ij}]x_j = x_i \left\{ \sum_{jl} k_{jil}x_l + \sum_j [\Gamma_{ji}(z) + \xi_{ji}] \right\}, \quad (1)$$

where $x_i \equiv n_i/n$ is the abundance of atom or molecule i (where n is the total volume density of hydrogen nuclei, and n_i is the density of i), and where $k_{ijl}(T)$ are the (temperature-dependent) rate coefficients ($\text{cm}^3 \text{ s}^{-1}$) for chemical reactions between species j and l that lead to the production of i , and $\Gamma_{ij}(z)$ and ξ_{ij} are the photon and cosmic-ray destruction rates (s^{-1}) of species j with products i (Gredel et al. 1989; Roberge et al. 1991; Millar et al. 1991). The photodestruction rates depend on the incident FUV radiation field and on the cloud depth z (cm), and the cosmic-ray destruction rates depend on the cosmic-ray hydrogen ionization rate. In our model we adopted an interstellar cosmic-ray H₂ ionization rate $\zeta = 5 \times 10^{-17} \text{ s}^{-1}$. In the Appendix we discuss the basic photochemical data we used in our calculations.

The chemical networks that govern the hydrogen, oxygen, carbon, sulfur, nitrogen, and silicon chemistry are shown in Figures 1–6 (Dalgarno & Black 1976; Prasad & Huntress 1979; van Dishoeck & Black 1986; van Dishoeck 1988; Millar et al. 1991). The dominant formation and destruction reactions and reaction pathways that lead to the synthesis of the atomic and molecular species vary with the cloud depth as the local radiation field and gas temperature vary. We describe these processes in detail in § 3.

TABLE 1
MODEL PARAMETERS

Parameter	Symbol	Value
Hydrogen particle density	$n_T (\text{cm}^{-3})$	10^6
FUV intensity	χ	2×10^5
Oxygen abundance	[O]	6×10^{-4}
Carbon abundance	[C]	3×10^{-4}
Sulfur abundance	[S]	1×10^{-5}
Nitrogen abundance	[N]	1×10^{-4}
Silicon abundance	[Si]	1×10^{-6}
PAH abundance	[PAH]	1×10^{-7}
Turbulent Doppler width	$b (\text{km s}^{-1})$	2.0
Grain photoelectric threshold	$B_0 (\text{eV})$	8.0
H ₂ 1–0 vibrational critical density	$n_{\text{H}_2}^{\text{crit}} \text{cm}^{-3}$	5×10^4

With the exception of H₂ we neglect the possible formation and ejection of molecules from grain surfaces (Breukers 1991; Shalabiea & Greenberg 1994).

In pressure equilibrium equation (1) must be solved subject to the constraining equation

$$p = (n_{\text{H}} + n_{\text{H}_2})kT + \frac{B^2}{8\pi} + \frac{1}{2}\rho b^2 \quad (2)$$

where the total pressure p is the sum of the thermal, magnetic, and turbulent pressures, n_{H} and n_{H_2} are the atomic and molecular hydrogen gas densities, B is the magnetic field, ρ is the mass density, and b is the “turbulent” velocity parameter. In our model we assume that the gas pressure is dominated by a magnetic field which is frozen into the gas, so that the total hydrogen particle density $n_T \equiv n_{\text{H}} + n_{\text{H}_2}$ remains constant through the cloud (Sternberg & Dalgarno 1989).¹

In thermal equilibrium equation (1) must also be solved subject to the additional constraining equation

$$G(T) - L(T) = 0 \quad (3)$$

where $G(T)$ and $L(T)$ are the total local volume heating and cooling rates (ergs cm^{-3}), respectively. We explicitly computed the gas temperature in the outer cloud layers where the incident FUV radiation field dominates the gas heating by a combination of grain photoelectric emission, photoionization of “large molecules,” and collisional deexcitation of FUV-pumped hydrogen molecules (Tielens & Hollenbach 1985; Lepp & Dalgarno 1988; Sternberg & Dalgarno 1989). The gas is cooled by atomic and ionic fine-structure line emission, and molecular rotational and vibrational line emission. We discuss the heating and cooling processes that we included in our calculations in the Appendix. At large cloud depths where the heating rates are less certain we adopted a uniform gas temperature equal to 20 K.

In Table 1 we summarize the input model parameters that we adopted in our calculations.

¹ Note that $n = n_{\text{H}} + 2n_{\text{H}_2}$ and that $n_T = n_{\text{H}} + n_{\text{H}_2}$ so that $n \neq n_T$.

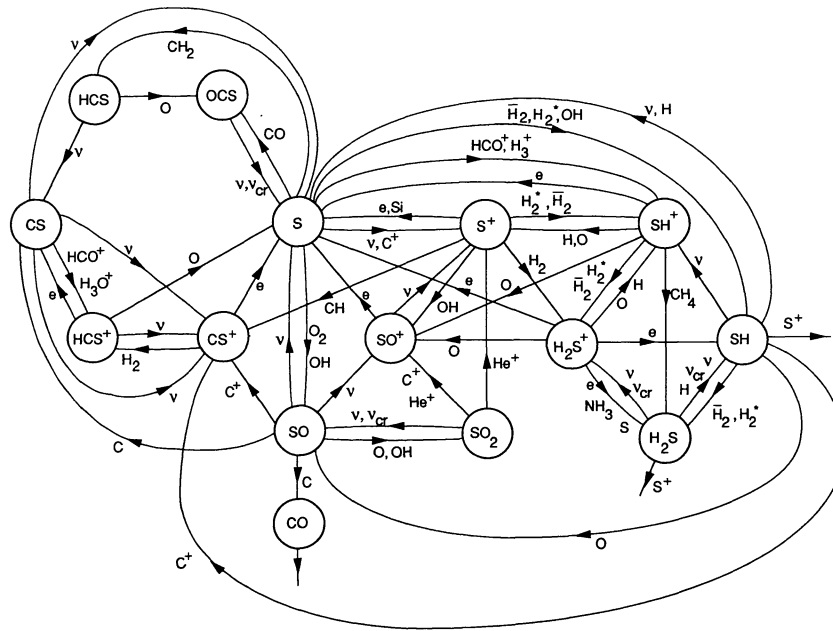


FIG. 4.—Sulfur network

“self-shielding” and dust opacity. The cloud depth at which the hydrogen becomes molecular depends on the ratio χ/n_T (Sternberg 1988), and in our model the atomic and molecular hydrogen densities become equal at a depth $A_V = 0.7$ from the cloud surface (see Fig. 8). We discuss our treatment of H₂ self-shielding and grain-surface formation in the Appendix.

As is shown in Figure 7 the gas in the H I zone is hot, with temperatures exceeding 10³ K. The H I zones in dense PDRs become hot because gas heating (by grain photoelectric emission, and collisional deexcitation of FUV-pumped H₂) becomes efficient while emission-line cooling is quenched (Sternberg & Dalgarno 1989; Burton et al. 1990). The gas remains hot through the outer part of the H/H₂ transition layer, but cools rapidly as the hydrogen becomes fully molecular.

The molecular chemistry in the hot H I zone and in the hot part of the H/H₂ transition layer is driven by rapid photoion-

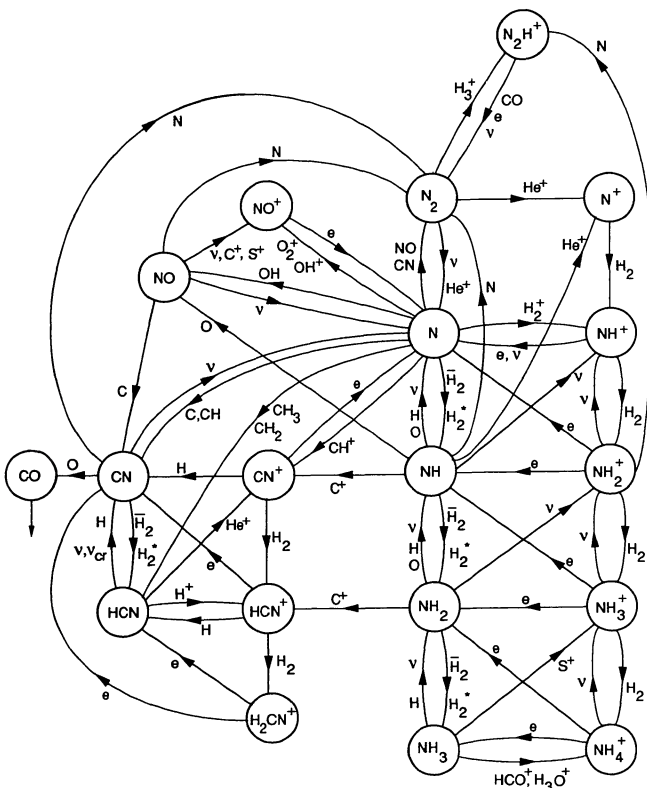


FIG. 5.—Nitrogen network

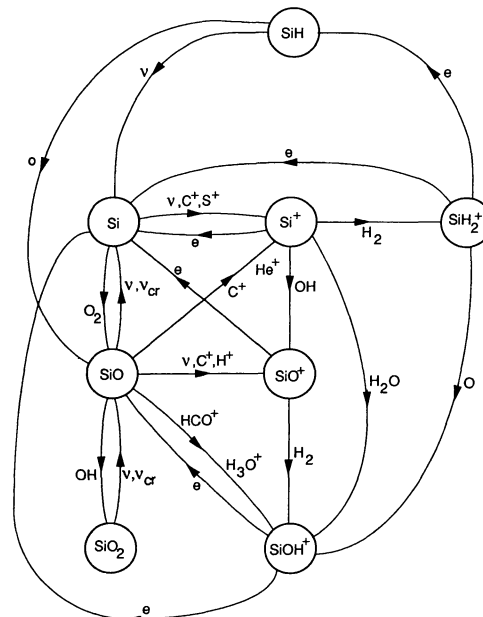


FIG. 6.—Silicon network

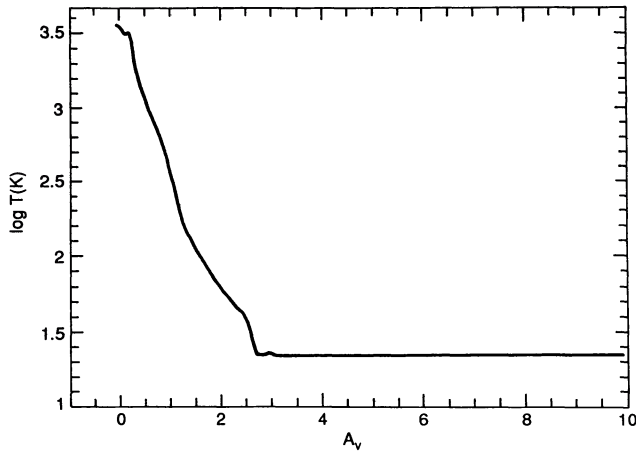


FIG. 7.—Thermal profile of the model cloud

ization and photodissociation and by FUV heating of the gas. The chemistry is initiated by several endothermic reactions between the hydrogen molecules and the abundant atoms and ions (C^+ , N , O , and S^+) which are produced by the rapid photoionization and photodissociation. These reactions become particularly effective in the H/H_2 transition region where the H_2 particle density becomes large but where the gas is still sufficiently warm for the reactions to proceed efficiently. A population of (superthermal) vibrationally excited hydrogen molecules is maintained by rapid FUV-pumping in the $H\ I$ zone, and the internal energies of these molecules may also be used to overcome the endothermicities of the mediating hydrogen abstraction reactions (see Appendix).

The incident FUV radiation field is not significantly attenuated in the $H\ I$ zone and in the H/H_2 transition layer, and the hot gas chemistry is moderated by rapid molecular photodissociation and photoionization. A large electron density, $n_e \sim 10^{-4}n_T$, is maintained in the $H\ I$ zone by the photoionization of atomic carbon, and the chemistry is also moderated by rapid dissociative recombination of the molecular ions.

Photodissociation of molecular ions becomes important in the outer layers of PDRs when $\chi/n_T \gtrsim 0.1\text{ cm}^3$ since, typically, the photodissociation rates are equal to $\sim 10^{-10}\chi\text{ s}^{-1}$ and the dissociative recombination rates are equal to $\sim 10^{-7}n_e\text{ s}^{-1}$. Thus, in the $H\ I$ zone of our model cloud photodissociation and dissociative recombination are competitive processes for the removal of the molecular ions.

3.1.1. Oxygen Family

Rapid molecular photodestruction maintains most of the oxygen in atomic form throughout the hot $H\ I$ zone and the H/H_2 transition layer, and the oxygen chemistry is initiated by the endothermic abstraction reaction



and by

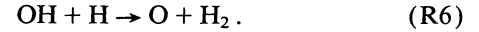


where in reaction (R4) H_2^* represents FUV-pumped hydrogen

molecules whose vibrational energies are used to overcome the endothermicity of reaction (R3). The OH molecules produced by reactions (R3) and (R4) are rapidly removed by photodissociation



and the reverse of reaction (R3)



The OH density increases as the H_2 density increases, and the formation reaction (R3) becomes very rapid in the outer part of the H/H_2 transition region. However, as the hydrogen becomes fully molecular, and the gas cools, reaction (R3) becomes ineffective while the OH photodissociation rate remains high and the OH density decreases sharply. In our model the OH abundance reaches a maximum value of 6×10^{-6} at a visual extinction $A_v = 0.6$ where $n(H_2)/n = 0.2$ and the gas temperature $T = 800\text{ K}$ (see Figs. 7 and 9). The OH radical is a crucial intermediary in the chemistry of the hot gas, and its very large abundance in the H/H_2 transition layer leads to the efficient production of many molecules and molecular ions in this part of the cloud.

H_2O is produced in the hot gas by



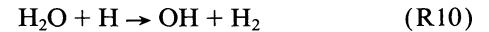
a reaction which possesses a large activation barrier, and by



and is rapidly removed by photodissociation



and the reverse of reaction (R7)



in the $H\ I$ zone where the atomic hydrogen density is large.

O_2 is efficiently produced by the fast neutral reaction

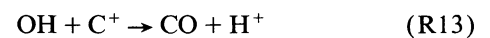


and is destroyed by photodissociation



throughout the $H\ I$ zone.

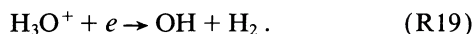
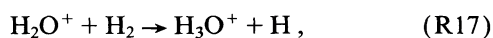
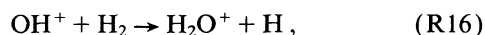
A crucial reaction in the $H\ I$ zone and in the H/H_2 transition layer is



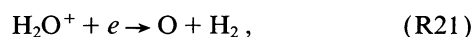
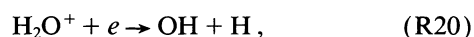
which is the major source of protons in the hot gas. The protons are removed by the charge transfer reaction



which initiates the sequence



The dissociative recombination of H_3O^+ is a negligible source of H_2O in the hot gas. In the H I zone where the H_2 density is small and the electron density is large the sequence of abstraction reactions (R15)–(R17) is interrupted by the dissociative recombinations



and



Photodissociation of H_2O^+ and H_3O^+ may be important processes in the hot gas. For example,



followed by



may be major sources of H_3^+ ions in the H I and H/ H_2 transition layers. Although the H_3^+ ions are rapidly removed by the dissociative recombinations



and

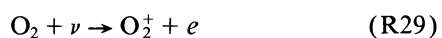


a large H_3^+ density may be maintained in the H/ H_2 transition layer by reactions (R23), (R24), and (R25).

O_2^+ is produced in the H I zone by



and by photoionization



and is removed by dissociative recombination



and photodissociation



The sequence (R14)–(R17) and reactions (R7), (R11), and (R28) maintain large densities of OH^+ , H_2O^+ , H_3O^+ , H_2O , O_2 , and O_2^+ near the OH density peak in the H/ H_2 transition layer (see Figs. 9 and 10).

3.1.2. Carbon Family

Rapid molecular photodestruction of the carbon bearing molecules and the photoionization of atomic carbon



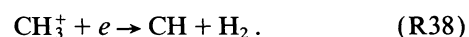
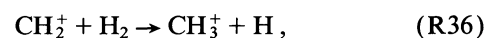
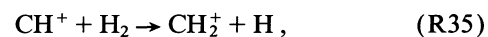
maintain most of the carbon in singly ionized form throughout the H I zone and the H/ H_2 transition layer, and the carbon chemistry is initiated by the endothermic abstraction reaction



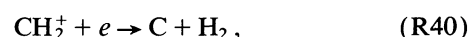
and by



The rapid formation of CH^+ by reactions (R33) and (R34) initiates the sequence



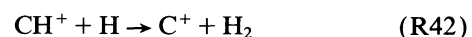
This sequence is interrupted by the dissociative recombinations



and



in the H I zone. The CH^+ ions formed by reactions (R33) and (R34) are removed by reactions (R35) and (R41), and also by the reverse of reaction (R33)

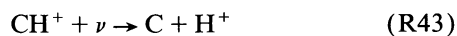


in the H I zone where the atomic hydrogen density is large.

A large CH^+ density peak is produced by reaction (R33) in the hot part of the H/ H_2 transition layer, and in our model the CH^+ abundance reaches a maximum value of 6×10^{-8} close to the location of the OH density peak (see Fig. 12). CH^+ , like OH, is also an important intermediary in the hot gas chemistry,

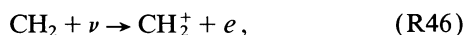
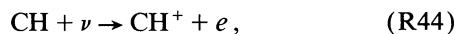
and its large abundance leads to the efficient production of several molecular species in the H/H₂ transition layer.

Near the CH⁺ density peak the dissociative recombination (R41) is the dominant source of atomic carbon, and the photodissociation of CH⁺

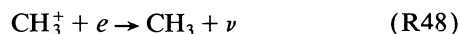


is a major source of protons.

The molecules CH and CH₂ are produced by reactions (R37), (R38), and (R39), and are removed by photoionization and photodissociation



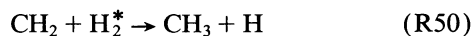
CH₃ is produced by radiative recombination



and by the endothermic abstraction reaction

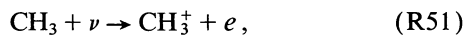


and by

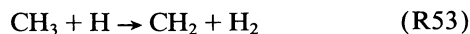


in the H I zone.

The CH₃ molecules are removed by photoionization and photodissociation

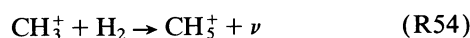


and by the reverse of reaction (R49)

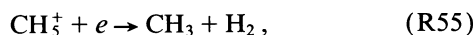


in the H I zone.

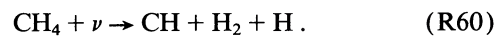
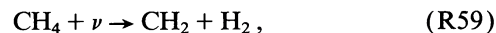
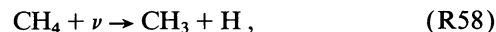
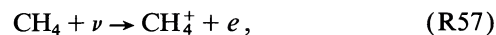
CH₄ is produced by radiative association



followed by



The dissociative recombination of CH₅⁺ is a negligible source of CH₃ in the hot gas. The CH₄ molecules are rapidly removed by photoionization and photodissociation



The sequence (R35)–(R38) and reactions (R48), (R49), (R50), (R54), and (R56) maintain large densities of CH₂⁺, CH₃⁺, CH, and CH₂ and smaller densities of CH₅⁺, CH₃, and CH₄ near the CH⁺ density peak in the hot part of the H/H₂ transition layer (see Figs. 12 and 13).

3.1.3. Sulfur Family

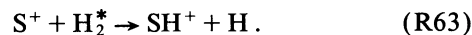
Rapid photodestruction of the sulfur bearing molecules and the photoionization of atomic sulfur



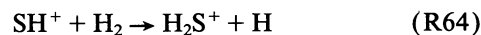
maintains most of the sulfur in singly ionized form throughout the H I zone and the H/H₂ transition layer, and the sulfur chemistry is initiated by the endothermic reaction



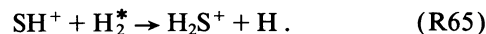
and by



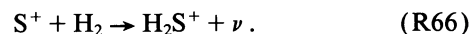
The formation of SH⁺ is followed by another endothermic reaction



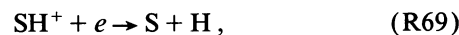
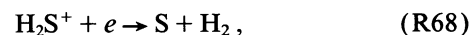
and by



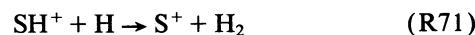
The production of H₂S⁺ by the sequence of endothermic reactions (R62) and (R64) is inefficient and is augmented by the radiative association



The SH⁺ and H₂S⁺ ions are removed by



and by the reverses of reactions (R62) and (R64)



in the H I zone. The dissociative recombination of SH⁺ is the

dominant source of atomic sulfur in the warm part of the H/
H₂ transition zone.

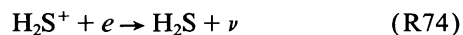
SH is formed by reaction (R67) and also by the endothermic
reaction



and



H₂S is produced by radiative recombination



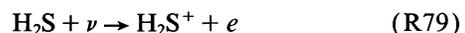
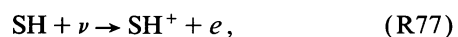
and by the endothermic reaction



and



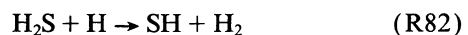
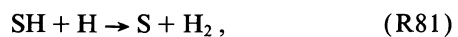
The SH and H₂S molecules are removed by photoionization
and photodissociation



and



and by the reverses of reactions (R72) and (R75)



in the H I zone.

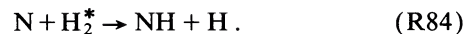
Because reaction (R62) is endothermic and the abundance
of atomic sulfur is very small in the H I zone, the formation
of SH by reactions (R67), (R72), and (R73), and of H₂S by
reactions (R74), (R75), and (R76) is inefficient, and only very
small densities of SH and H₂S are maintained in the hot gas
(see Fig. 15).

3.1.4. Nitrogen Family

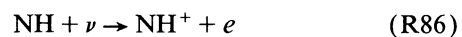
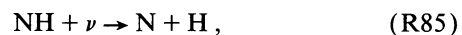
Rapid photodestruction of the nitrogen bearing molecules
maintains most of the nitrogen in atomic form throughout the
H I zone and H/H₂ transition layer, and the nitrogen chemis-
try is initiated by the endothermic abstraction reaction



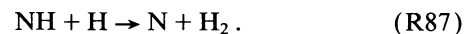
and by



The NH molecules formed by reactions (R83) and (R84) are
removed by photodissociation and photoionization

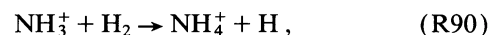
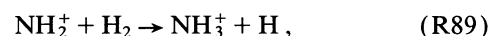
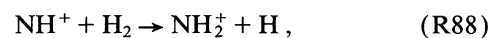


and by the reverse of reaction (R83)

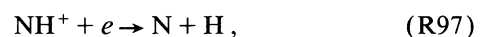
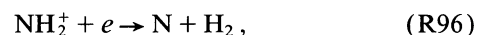
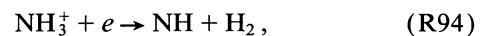
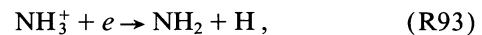


The photodissociation of NH is the dominant source of atomic
nitrogen in the hot gas.

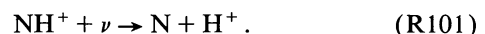
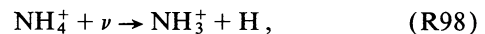
The photoionization of NH initiates the sequence



In the H I zone this sequence is interrupted by the dissociative
recombinations



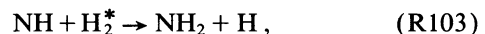
and also by the photodissociations



NH₂ is produced by reactions (R92) and (R93) and also by
the endothermic reaction



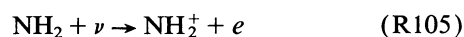
and by



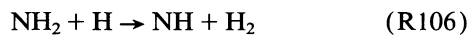
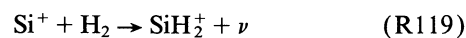
and is removed by photodissociation and photoionization



maintain most of the silicon in singly ionized form throughout the H I zone and the H/H₂ transition layer. The silicon chemistry is initiated by radiative association

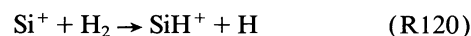


and by the reverse of reaction (R102)



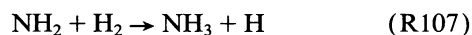
rather than by the hydrogen abstraction

in the H I zone.

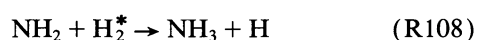
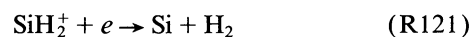


NH₃ is produced by reaction (R91) and by the endothermic reaction

because reaction (R120) is extremely endothermic and remains ineffective even in the hot gas. Reaction (R119) is followed by

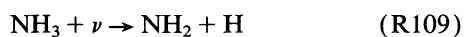


and by



and

and is removed by photodissociation



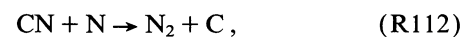
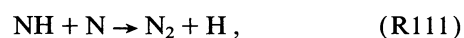
SiH is formed by reaction (R122) and is removed by photodissociation

and the reverse of reaction (R107)



Because the silicon chemistry is initiated by radiative association the production of SiH by reaction (R122) is inefficient, and radiative recombination

N₂ is produced by the reactions



rather than the dissociative recombination of SiH₂⁺ is the major source of atomic silicon in the hot gas. Only a very small SiH density is maintained in the H I zone and in the H/H₂ transition layer (see Fig. 18).

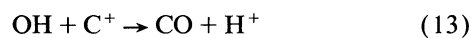
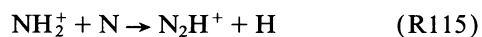
and is removed by photodissociation



3.1.6. Oxygen Intermediates

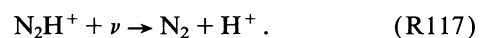
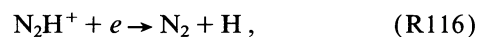
N₂H⁺ is produced by

CO is efficiently produced in the hot gas by the reaction

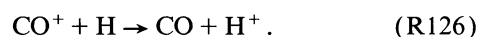


and is removed by dissociative recombination and photoionization

and by

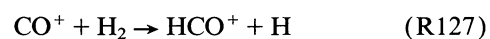


followed by



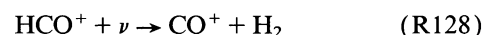
Reactions (R83), (R102), and (R107), and the sequence (R88)–(R92), maintain large densities of NH, NH⁺, NH₂⁺, NH₃⁺, NH₄⁺, NH₂, and NH₃ in the hot part of the H/H₂ transition layer. However, the densities of N₂ and N₂H⁺ remain very small in the hot gas (see Figs. 19, 20, and 21).

HCO⁺ is produced by

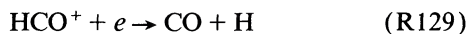


and is removed by photodissociation

Rapid photodestruction of the silicon bearing species and the photoionization of atomic silicon



and dissociative recombination



which is an additional source of CO in the hot gas. The CO molecules are removed by photodissociation



Reaction (R13) and the sequence (R125)–(R129) maintain large densities of CO, CO⁺, and HCO⁺ near the OH density peak in the H/H₂ transition region (see Fig. 11).

SO⁺ is efficiently produced by the reaction



and is removed by dissociative recombination



and photodissociation



A large density of SO⁺ is maintained in the H/H₂ transition layer, and the dissociative recombination of SO⁺ is the dominant source of atomic sulfur in the hot gas (see Fig. 14).

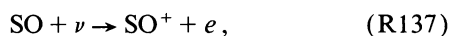
SO and SO₂ are produced by



and



and are removed by photodissociation and photoionization



However, because the density of atomic sulfur is very small in the H I zone and in the H/H₂ transition layer only very small densities of SO and SO₂ are maintained in these cloud layers (see Fig. 14).

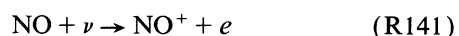
NO is efficiently produced by



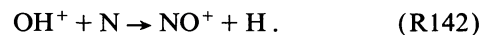
and is removed by photodissociation



and photoionization



which is the major source of NO⁺ in the hot gas. An additional source is

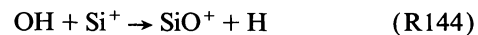


The NO⁺ ions are removed by

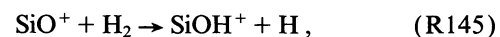


Reactions (R139), (R141), and (R142) maintain large densities of NO and NO⁺ near the OH density peak in the H/H₂ transition region (see Figs. 19 and 21).

SiO⁺ is produced rapidly by the reaction



which initiates the sequence

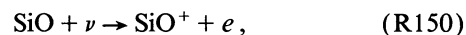


This sequence is interrupted by the dissociative recombination

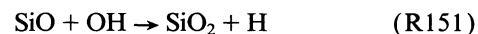


in the H I zone. This reaction is a major source of silicon atoms in the hot gas.

SiO is produced by reaction (R147) and is removed by photodissociation and photoionization



and SiO₂ is produced by



and is removed by photodissociation



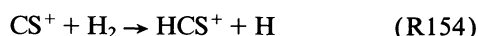
A moderate SiO density is maintained near the OH density peak in the H/H₂ transition layer. However, the density of SiO₂ remains negligible in this part of the cloud (see Fig. 17).

3.1.7. Carbon Intermediates

CS⁺ is rapidly produced by the reaction



which is followed by



and



This sequence is interrupted by dissociative recombination



and photodissociation



CS is produced by reaction (R155) and is removed by photodissociation and photoionization

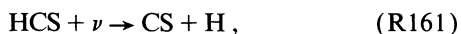


Reactions (R153)–(R155) produce CS, CS⁺, and HCS⁺ density peaks near the CH density peak in the H/H₂ transition layer (see Fig. 16).

HCS is inefficiently produced by



and is rapidly destroyed by photodissociation



and only a small density of HCS is maintained in the hot gas.

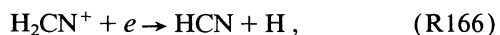
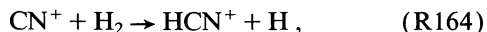
CN⁺ is formed by



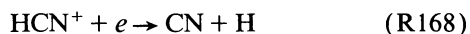
and



These reactions initiate the sequence



which is interrupted by the dissociative recombinations



and

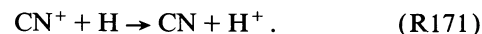


in the H I zone.

CN is produced by reactions (R167) and (R168) as well as by



and



HCN is produced by reaction (R166), by the reactions



and



by the endothermic reaction



and by



The CN and HCN molecules are removed by photodissociation



and



throughout the H I zone and the H/H₂ transition layer. The HCN molecules are also removed by the reverse of reaction (R174)



in the H I zone where the atomic hydrogen density is large.

Reactions (R162)–(R175) maintain large densities of CN⁺, HCN⁺, CN, and HCN near the CH density peak in the H/H₂ transition layer (see Fig. 22).

3.2. C II and S II Zones

The photoionization of atomic carbon



by the incident FUV field maintains an extended cloud layer in which most of the carbon is singly ionized. This layer extends deeper into the cloud than does the H I zone because of the effective self-shielding of the hydrogen molecules. Thus, a C II zone exists in which most of the carbon is singly ionized and in which the hydrogen is fully molecular. In our model such a C II zone is present at cloud depths between $A_V = 0.7$ and $A_V = 1.7$ (see Figs. 8 and 11).

Similarly, the photoionization of atomic sulfur



as well as the charge transfer reaction



maintains an extended cloud layer in which most of the sulfur is singly ionized. This layer extends to larger cloud depths than does the layer of ionized carbon because sulfur is less abundant than carbon. Thus a S II zone exists in which the sulfur is singly ionized but in which the carbon is neutral (and present primarily in CO molecules), and in which the hydrogen is fully molecular. In our model such a S II zone is present at cloud depths between $A_V = 1.7$ and $A_V = 3.7$ (see Figs. 8, 11, and 14).

The molecular chemistry in the C II and S II zones is driven by photoionization and photodissociation, and is initiated by radiative association and abstraction reactions between the hydrogen molecules and the abundant atoms and ions O, N, C⁺, Si⁺, and S⁺. The endothermic hydrogen abstraction reactions (R3), (R33), (R62), and (R83) which control the molecular production in the hot H I zone and H/H₂ transition layer become much less effective in the C II and S II zones where the gas is cold with temperatures $T \lesssim 100$ K (see Fig. 7), and proceed only in reactions with FUV pumped H₂^{*} molecules.

The FUV radiation field is partially attenuated in the C II and S II zones, but the chemistry is still moderated by rapid molecular photodissociation and photoionization throughout these cloud layers. Electrons are produced by the photoionizations (R32) and (R61), and dissociative recombination remains rapid in the C II and S II zones.

3.2.1. Oxygen Family

FUV-pumping maintains a population of vibrationally excited hydrogen molecules throughout the C II and S II zones, and the formation of OH is dominated by



even at the inner edge of the S II zone where the density of vibrationally excited hydrogen molecules becomes very small. In the S II zone additional sources of OH are



and



The OH molecules are removed by photodissociation



throughout the C II and S II zones. Near the inner edge of the C II zone where the FUV radiation field is partially attenuated, but where the C⁺ density is still large, the OH molecules are also effectively removed by



and by

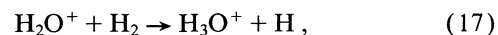
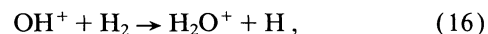


Reaction (R13) continues to dominate the production of protons in the C II zone.

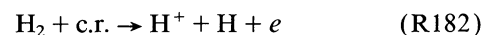
The protons are removed by



which in the C II zone continues to initiate the sequence



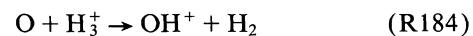
In the S II zone, the C⁺ density becomes small and the protons are produced by cosmic-ray dissociative ionization



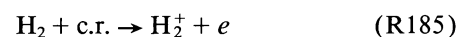
rather than by reaction (R13). In the cold S II zone the protons are removed by radiative recombination



rather than by the charge transfer reaction (R14) which is endothermic. The proton density becomes small in the S II zone, and the hydrogen abstraction sequence (R16)–(R19) is initiated by the proton transfer reaction



(rather than by reaction [R14] followed by [R15]) where the H₃⁺ ions are produced by cosmic-ray impact ionization



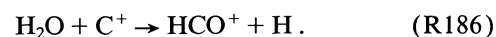
followed by



H₂O is formed by the dissociative recombination of H₃O⁺ and is removed by photodissociation



throughout the C II and S II zones. Near the inner edge of the C II zone the H₂O molecules are also removed by



O₂ is formed by

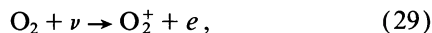


and is removed by photodissociation



throughout the C II and S II zones.

O_2^+ is formed and destroyed by



and



throughout the C II and S II zones.

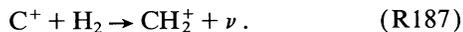
The formation of molecular species of the oxygen family is less efficient in the cool C II and S II zones than in the hot H I zone and H/H₂ transition layer (see Figs. 9 and 10).

3.2.2. Carbon Family

The carbon chemistry in the C II zone is initiated by the combined action of

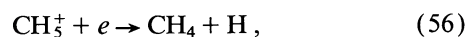
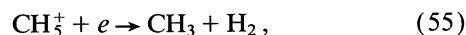
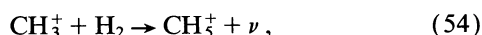
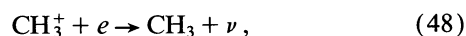
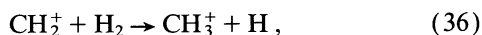
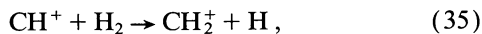


and the radiative association reaction

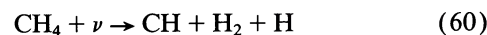
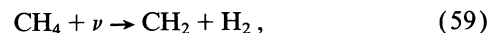
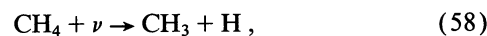
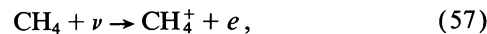
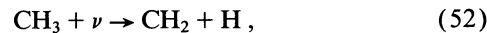
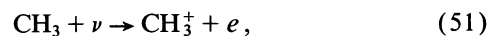
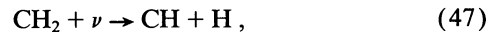
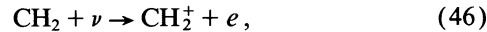
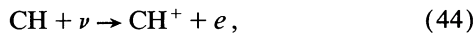


In the S II zone where the density of FUV-pumped molecules is very small the carbon chemistry is controlled primarily by reaction (R187).

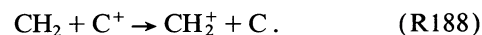
Reactions (R34) and (R187) are followed by the sequence



which leads to the formation of CH, CH₂, CH₃, and CH₄. These molecules are removed by photodissociation and photoionization

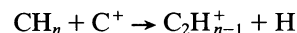


throughout the C II and S II zones. Near the inner edge of the C II zone the CH₂ molecules are also removed by



CH₃ is formed in the C II and S II zones both by reactions (R48) and (R55), as well as by the photodissociation of CH₄.

The carbon hydrides are also removed by carbon insertion reactions of the form



near the inner edge of the C II zone. These reactions will lead to the efficient production of complex hydrocarbons in this part of the cloud.

Radiative recombination



is the dominant source of neutral atomic carbon in the C II zone. A large density of atomic carbon is maintained near the inner edge of the C II zone by reaction (R189) where the rate of carbon photoionization is reduced but where the carbon bearing molecules are still being destroyed by the FUV radiation field. In the S II zone where the C⁺ density is small the dominant source of carbon is



rather than reaction (R189).

The densities of the molecular ions CH⁺, CH₂⁺, CH₃⁺, and CH₅⁺ decrease through the C II and S II zones as the densities of FUV-pumped H₂ molecules and C⁺ ions decrease. The densities of CH, CH₂, CH₃, and CH₄ increase with increasing depth through the C II zone as the destructive FUV radiation field is attenuated. However, the densities of these molecules decrease through the S II zone as the C⁺ density decreases and the initiating reaction (R187) proceeds more slowly (see Figs. 12 and 13).

3.2.3. Sulfur Family

Sulfur ions are produced by the charge transfer reaction

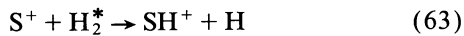


and by photoionization

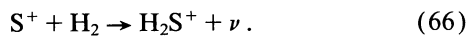


in the C II and S II zones. Reaction (R179) dominates the production of S^+ in the C II zone where the C^+ density is large, and reaction (R61) dominates in the S II zone where the C^+ density is small.

The sulfur chemistry in the C II and S II zones is initiated by the combined action of

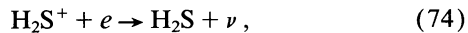
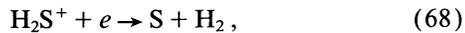
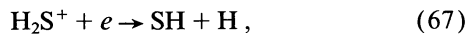
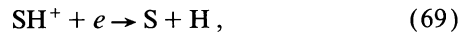


and radiative association

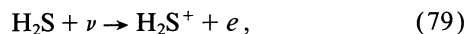
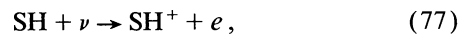


Reaction (R63) is less effective in the S II zone where the density of FUV-pumped hydrogen molecules is very small.

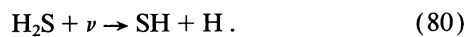
Reactions (R63) and (R66) are followed by the sequence



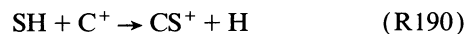
and the SH and H_2S molecules that are formed by this sequence are removed by photoionization and photodissociation



and

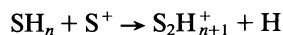


The SH molecules are also removed by



near the inner edge of the C II zone.

The hydrogen sulfides are also removed by sulfur insertion reactions of the form



near the inner edge of the S II zone. These reactions will lead to the efficient production of complex hydrosulfides in this part of the cloud.

The production of SH^+ and H_2S^+ and the reaction sequence (R69)–(R74) proceeds more slowly in the C II and S II zones than in the H I zone. The dominant source of atomic sulfur in these cloud layers is therefore radiative recombination



rather than the dissociative recombination of SH^+ .

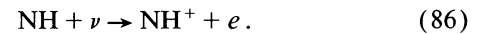
The densities of SH and H_2S increase through the C II and S II zones as the destructive FUV radiation field is attenuated with increasing cloud depth (see Fig. 15).

3.2.4. Nitrogen Family

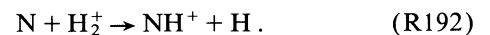
Photodestruction of the nitrogen bearing molecules maintains most of the nitrogen in atomic form throughout the C II and S II zones. The nitrogen chemistry is mediated by



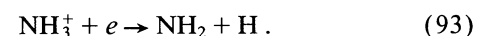
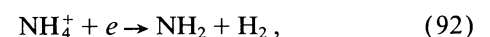
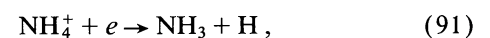
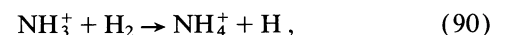
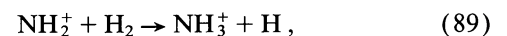
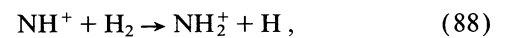
followed by



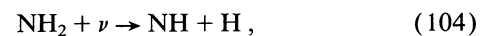
In the S II zone where the density of FUV-pumped H_2 becomes small the production of NH^+ is augmented by



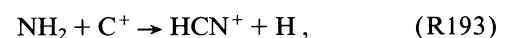
Reactions (R86) and (R192) initiate the sequence



The NH_2 and NH_3 molecules that are produced by this sequence are removed by photodissociation and photoionization



throughout the C II and S II zones. Near the inner edge of the C II zone the NH_2 molecules are also removed by



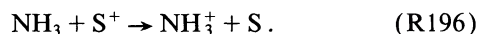
and near the inner edge of the S II zone, where the radiation field is attenuated, the NH , NH_2 , and NH_3 molecules are also removed by the fast neutral reactions



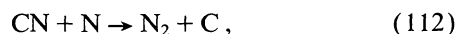
and



and by the charge transfer reaction



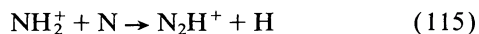
In the C II zone the production of N_2 is dominated by the reaction



and in the S II zone by the reaction

The N_2 molecules are removed by photodissociation

throughout the C II and S II zones. N_2H^+ ions continue to be produced by



in the C II zone. In the S II zone these ions are produced by

The N_2H^+ ions are removed by dissociative recombination

throughout the C II and S II zones.

With the exception of N_2 the formation of molecular species of the nitrogen family is less efficient in the C II and S II zones than in the hot H I zone and H/ H_2 transition layer (see Figs. 19, 20, and 21).

3.2.5. Silicon Family

Silicon ions are produced by photoionization



throughout the C II and S II zones. Additional sources of Si^+ ions are the charge transfer reactions

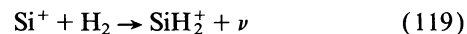


near the inner edge of the C II zone, and

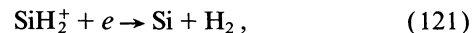
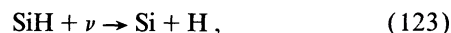


in the S II zone. Most of the silicon remains in singly ionized form throughout the C II and S II regions.

SiH is produced by the radiative association reaction



followed by

The SiH molecules are removed by photodissociation

and the SiH density increases with increasing cloud depth through the C II and S II zones as the photodestruction rate decreases (see Fig. 18).

3.2.6. Oxygen Intermediates

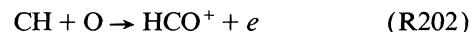
Atomic oxygen remains abundant in the C II and S II zones and CO is produced by the reactions



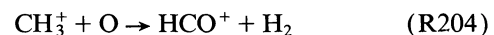
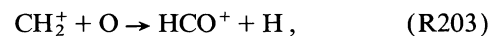
and



rather than by reactions (R13) or (R123). Chemi-ionization



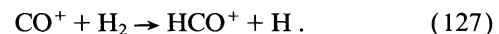
and the reactions



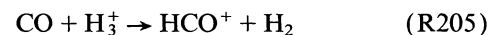
are major sources of HCO^+ in both the C II and S II zones. In the C II zone HCO^+ is also produced by



followed by



Near the inner edge of the S II zone the reaction



becomes the dominant source of HCO^+ . The HCO^+ ions are removed by dissociative recombination

and reaction (R127) dominates the removal of the CO^+ ions

throughout the C II and S II zones. The CO molecules are removed by photodissociation



in the C II and S II zones. The CO^+ and HCO^+ densities become small in the C II and S II zones. The CO density becomes large near the inner edge of the C II zone as all of the gas-phase carbon is driven into the CO molecules (see Fig. 11).

In the C II zone SO^+ is produced by



and is removed by



and SO and SO_2 are produced by



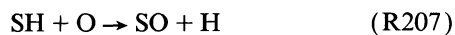
and



An additional source of SO_2 in the C II zone is the radiative association



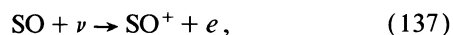
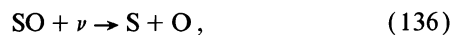
In the S II zone SO and SO^+ are produced by



and



rather than by reactions (R134) and (R131) because the OH density becomes small. The production of SO_2 is dominated by reaction (R206) in the S II zone. The SO and SO_2 molecules are removed by photodissociation and photoionization



throughout the C II and S II zones, and the densities of these molecules increase with increasing cloud depth as the photo-destruction rates diminish (see Fig. 14).

NO is produced in the C II and S II zones by



and by



and is removed by photodissociation and photoionization



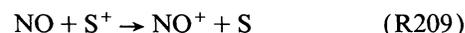
The NO molecules are also removed by



near the inner edge of the C II zone, and by



in the S II zone. Reactions (R141) and (R209) are the dominant sources of NO^+ in the C II zone. In the S II zone NO^+ ions are formed by

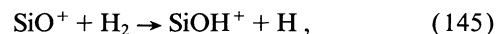


and are removed by

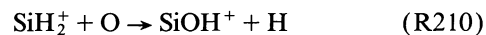


The NO density is limited by reactions (R208) and (R113) and remains approximately constant through the C II and S II zones (see Fig. 19).

SiO is produced in the C II zone by the sequence



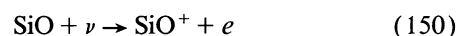
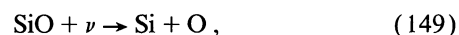
In the S II zone the production of SiO is augmented by



followed by reaction (R147) and by



The SiO molecules are removed by photodissociation and photoionization



throughout the C II and S II zones and also by

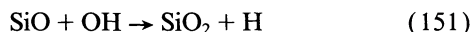


and



near the inner edge of the C II zone.

SiO₂ is inefficiently produced by



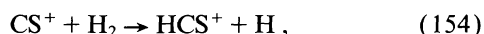
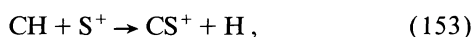
and removed by photodissociation



The SiO density increases with increasing cloud depth as the rates of photo- and chemical destruction by reactions (R149), (R150), (R212), and (R213) decrease. The SiO₂ density remains negligible in the C II and S II zones (see Fig. 17).

3.2.7. Carbon Intermediates

The carbon-sulfur intermediates CS⁺, HCS⁺ and CS are produced by the sequence



in the C II and S II zones. The CS molecules formed by reaction (R155) are removed by photodissociation and photoionization



The CS density increases toward the inner edge of the C II zone as the photodestruction rates diminish, but decreases through the C⁺/C/CO transition region as the electron density and the rate of reaction (R155) decrease (see Fig. 16).

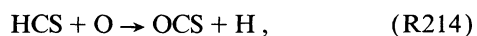
HCS is formed by



and destroyed by photodissociation



In the S II zone the HCS molecules are also removed by



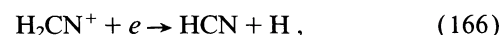
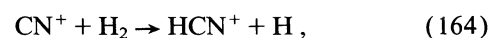
and the OCS molecules formed by reaction (R214) are removed by



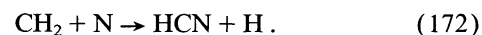
The formation of the carbon-nitrogen intermediates in the C II and S II zones is initiated by



followed by the sequence



The formation of HCN in the C II and S II zones is augmented by the reaction



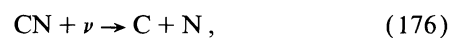
The HCN molecules are removed by photodissociation



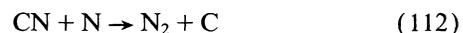
which together with reaction (R177) and



are the major sources of CN. The CN molecules are removed by photodissociation



and by



near the inner edge of the S II zone.

The CN density becomes large near the edge of the C II zone where the reaction sequence (R162)–(R167) remains effective, but where the rate of photodestruction by reaction (R176) is diminished. The CN density decreases through the S II zone as the C⁺ density decreases. The CN/HCN density ratio is large throughout the C II and S II zones (see Fig. 22).

3.3. Si II and S I Zones

The photodissociation of atomic silicon



and the charge transfer reaction



maintain a cloud layer in which most of the silicon is singly ionized. Because of the small silicon abundance this layer extends to larger cloud depths than the ionized carbon or sulfur layers. Thus, a Si II zone exists in which the silicon is ionized, but in which the carbon and sulfur are present in neutral (atomic or molecular) form, and in which the hydrogen is fully molecular. In our model a Si II zone is present at cloud depths between $A_V = 3.7$ and 6 (see Figs. 8, 11, 14, and 17).

At intermediate cloud depths a S I zone exists in which most

of the sulfur is present in neutral atomic form. The S I zone is maintained by photodestruction of the sulfur-bearing molecules, and rapid neutralization of the sulfur ions by radiative recombination

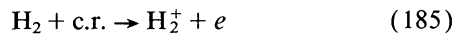


and the charge transfer reaction (R199). In our model a broad S I zone is present at cloud depths between $A_V = 3.7$ and 7.6, and the Si II and S I zones overlap (see Figs. 14 and 17).

The FUV radiation field is severely attenuated in the Si II and S I zones, and the chemistry is driven by a combination of photoionization and photodissociation and cosmic-ray ionization. The chemistry is initiated by radiative associations and proton transfer reactions. The electron density becomes small while the atomic oxygen density remains large, and reactions between the molecular ions and the oxygen atoms begin to compete with dissociative recombinations in the Si II and S I zone. The molecular chemistry is moderated by photodissociation and photoionization which proceeds more slowly in the Si II and S I zones than in the cloud layers closer to the surface.

3.3.1. Oxygen Family

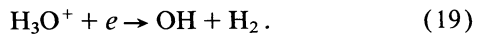
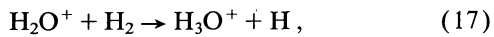
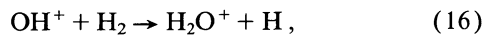
In the Si II and S I zones the oxygen chemistry is driven by cosmic-ray ionization



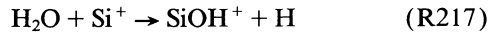
followed by



and the sequence



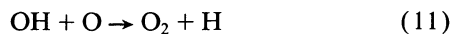
The dissociative recombinations (R18) and (R19) are the dominant sources of H_2O and OH in the Si II and S I zones. The H_2O molecules are removed by



and by photodissociation



which is an additional source of OH . The OH molecules are removed by



and the O_2 formed by reaction (R11) is removed by photodissociation



as well as by



and



O_2^+ is produced by



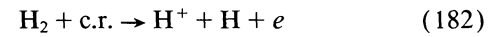
and by



and is removed by



Protons are produced by cosmic rays



and are removed by radiative recombination



in the Si II zone, and by the charge transfer reaction

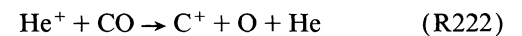


in the S I zone.

The O_2 and H_2O densities increase through the Si II and S I zones as the rates of photodestruction by reactions (R9) and (R12) decrease. However, the OH density is limited by reaction (R11) and approaches a constant value at large cloud depths (see Fig. 9).

3.3.2. Carbon Family

The dominant source of C^+ in the S I zone is the reaction



where the He^+ ions are produced by cosmic-ray ionization

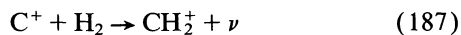


The C^+ ions are removed by the charge transfer reaction



which is the dominant source of atomic carbon in the S I zone.

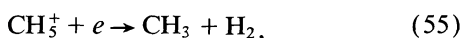
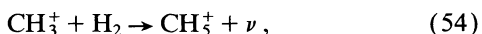
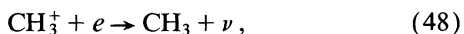
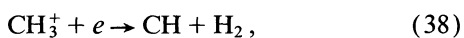
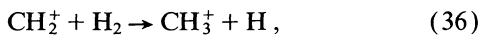
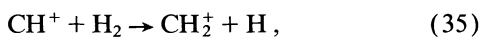
The carbon chemistry is initiated by the radiative association



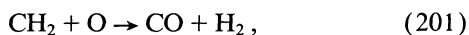
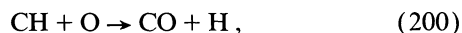
and also by the proton transfer reaction



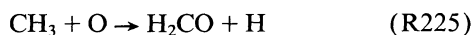
in the S I zone where the C^+ density becomes small. These reactions are followed by the sequence



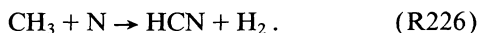
The CH , CH_2 radicals formed by this sequence are removed by the neutral reactions



and the CH_3 radicals are removed by³



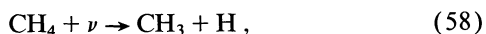
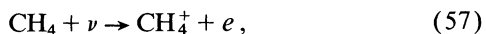
and by



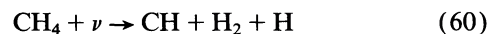
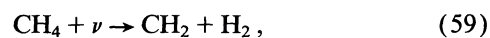
CH_4 is formed by the dissociative recombination (R56) and also by



The CH_4 molecules continue to be removed by photodissociation and photoionization



³ Although reaction (R225) dominates the removal of the CH_3 radicals in the Si II and S I zones and in the dark core (see below) we have not explicitly included it in our calculations since we have not considered the formation and destruction of H_2CO in our model.



throughout the Si II and S I zones, and by



near the inner edge of the S I zone where the radiation field is attenuated.

The CH_4 density increases through the cloud as the rates of photodestruction by reactions (R57)–(R60) diminish. However, the densities of CH^+ , CH_2^+ , CH_3^+ , CH_4^+ , CH_5^+ , CH , CH_2 , and CH_3 become very small in the Si II and S I zones (see Figs. 12 and 13).

3.3.3. Sulfur Family

S^+ is produced by photoionization



and charge transfer



in the Si II and S I zones. The sulfur ions are removed by radiative recombination

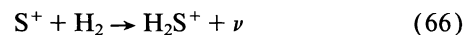


and also by the charge transfer reaction

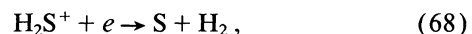


near the inner edge of the S I zone where the electron density becomes small.

H_2S^+ ions are produced by



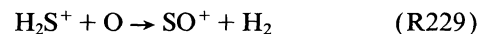
and are removed by dissociative recombination



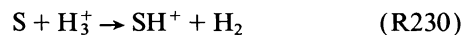
and also by reactions with atomic oxygen



and



near the inner edge of the S I zone. SH^+ is formed by the proton transfer reaction



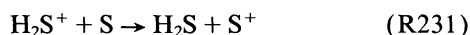
and removed by



SH is formed by reaction (R67) and is removed by



H₂S is efficiently produced by the charge transfer reaction



and is removed by photodissociation



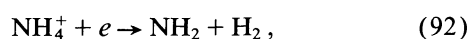
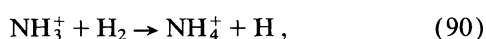
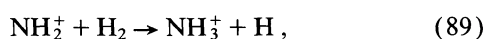
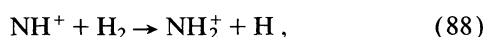
throughout the Si II and S I zones. A large H₂S density is maintained near the inner edge of the S I zone where the formation reaction (R231) remains efficient, but where the rate of photodestruction by reaction (R80) is reduced. The H₂S density drops sharply beyond the edge of the S I zone as the density of atomic sulfur decreases and the sulfur is driven into SO and SO₂. In our model the H₂S abundance reaches a maximum value of 6×10^{-9} at a visual extinction $A_V = 7.6$ (see Figs. 14 and 15).

3.3.4. Nitrogen Family

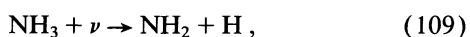
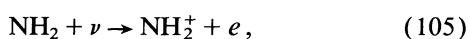
Nitrogen is fully molecular, and the nitrogen chemistry is driven by the reaction



which initiates the sequence



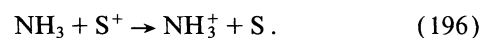
The NH₂ and NH₃ molecules produced by this sequence are removed by photodissociation and photoionization



and also by



and charge transfer



Reaction (R195) is the major source of NH in the S I zone. The NH molecules are removed primarily by

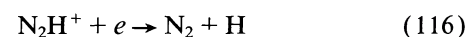


in the S I zone.

N₂H⁺ ions are produced by the reaction



and are removed by dissociative recombination



in the Si II and S I zones.

The NH₃ density increases through the Si II and S I zones as the rate of photodestruction by reaction (R109) decreases. However, the densities of NH and NH₂ are limited by reactions (R195), (R180), and (R194), and their abundances approach constant values (see Fig. 21). The density of N₂H⁺ ions increases with cloud depth as the electron density decreases (see Fig. 19).

3.3.5. Silicon Family

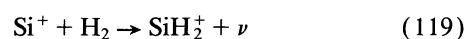
Si⁺ is produced by photoionization



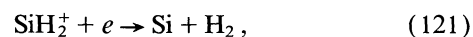
and by charge transfer



in the Si II and S I zones. SiH is produced by radiative association



followed by



The SiH molecules are removed by photodissociation



and also by



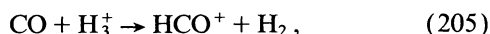
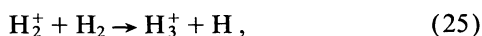
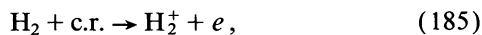
and



near the inner edge of the S I zone where the UV field is attenuated. The SiH density decreases beyond the edge of the Si II zone as the Si⁺ density decreases (see Fig. 18).

3.3.6. Oxygen Intermediates

HCO⁺ is produced in the S I zone by the sequence



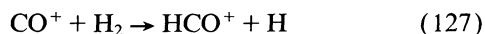
and is removed by



The HCO⁺ density increases with cloud depth as the electron density decreases (see Fig. 11). CO⁺ is very inefficiently produced by



and is rapidly removed by



and a negligible CO⁺ density is maintained in the S I zone.

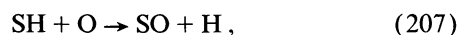
SO⁺ is produced by



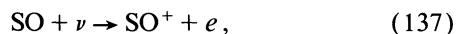
and is removed by



SO and SO₂ are produced by the reactions



and are removed by photodissociation and photoionization



and



Near the inner part of the S I zone the reactions



dominate the removal of the SO molecules. The SO and SO₂ densities and the SO₂/SO density ratio increase through the Si II and S I zone as the rates of photodestruction by reactions (R136), (R137), and (R138) decrease (see Fig. 14).

NO is produced by



and is removed by



which is the dominant source of N₂ in the Si II and S I zones. NO⁺ is inefficiently produced by

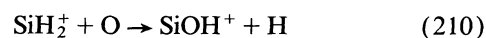


and is removed by

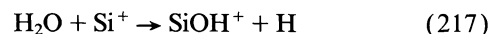


The NO density is limited by reaction (R113) and remains approximately constant through the Si II and S I zones (see Fig. 19).

SiO is produced by the reactions



and by



followed by



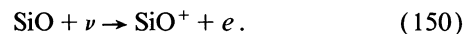
and



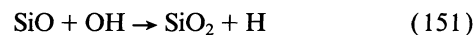
The dissociative recombination (R146) is a major source of OH in the S I zone. The SiO molecules are removed by photodissociation and photoionization



and



SiO₂ is produced by



and is removed by photodissociation



The SiO and SiO₂ densities increase with the cloud depth as the rates of photodestruction by reactions (R149), (R150), and (R152) diminish (see Fig. 17).

3.3.7. Carbon Intermediates

CS is formed by



and is removed by photodissociation and photoionization



The CS density becomes large near the inner edge of the S I zone where atomic carbon is still efficiently produced by the charge transfer reaction



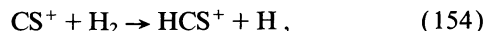
and where the rates of photodestruction by reactions (R158) and (R159) are diminished. The CS density drops sharply beyond the inner edge of the S I zone where reaction (R179) becomes an inefficient source of atomic carbon, and where the SO molecules are preferentially driven to SO₂ by reaction (R206). In our model the CS abundance reaches a peak value of 8.5×10^{-6} at a visual extinction $A_V = 8$ (see Fig. 16).

Near the CS density peak the photodissociation of CS is itself a major source of atomic carbon, and the charge transfer reaction

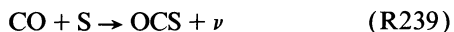


dominates the removal of the protons.

CS⁺ is formed primarily by reaction (R159) which is followed by



OCS is produced by



and removed by photodissociation



HCN is produced by the reactions



and



and is removed by photodissociation



CN is formed by reaction (R177) and also by



and



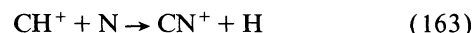
The CN molecules are removed by



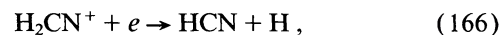
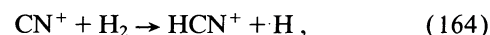
and



The formation of CN⁺ is dominated by



which initiates the sequence



However, reactions (R166) and (R167) are only minor sources of CN and HCN in the Si II and S I zones.

The HCN density increases and the CN density decreases with increasing cloud depth as the HCN photodestruction rate decreases (see Fig. 22).

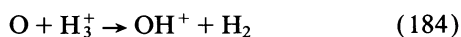
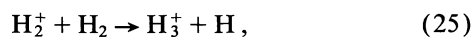
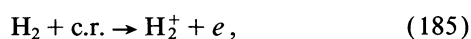
3.4. Dark Core

At sufficiently large cloud depths the incident FUV field is completely attenuated, and the external photons no longer dominate or influence the cloud chemistry. In our model the inner edge of the photon-dominated region occurs at a cloud depth $A_V \approx 10$. A dark cloud core exists at greater cloud depths where the chemistry is driven by cosmic-ray ionization of hydrogen and helium.

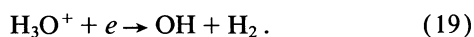
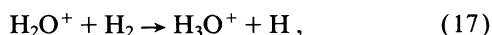
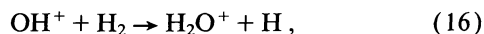
In our model the density of the nonreactive metal ions is small, and most of the positive electric charge is carried by the abundant molecular ions. The fractional ionization is much smaller in the dark core than in the PDR, and the abundances of saturated molecular ions become large. Neutral molecules are removed by fast ion-molecule reactions (Prasad & Huntress 1979) and also by cosmic-ray-induced photodissociation and photoionization (Prasad & Tarafdar 1983; Sternberg, Dalgarno, & Lepp 1987; Gredel, Lepp, & Dalgarno 1987; Gredel et al. 1989).

3.4.1. *Oxygen Family*

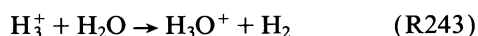
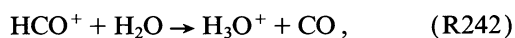
The oxygen chemistry in the dark core is (as in the Si II and S I zones) driven by cosmic-ray ionization and proton transfer in the sequence



followed by



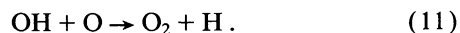
Reaction (R18) is the dominant source of H_2O which is removed by the reactions



and by cosmic-ray-induced photodissociation



OH is formed by reaction (R19) and is removed by



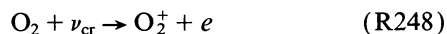
The O_2 formed by reaction (R11) is removed by



and by



O_2^+ ions are produced by cosmic-ray-induced photoionization



and by



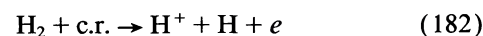
and are removed by



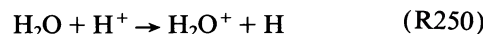
and



Protons are produced by cosmic rays



and are removed by reaction (R220) and by

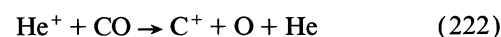


in the dark core.

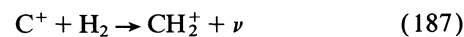
Atomic oxygen is produced by reactions (R245) and (R246) and is removed by reactions (R19) and (R184). Most of the oxygen remains atomic in the dark core (see Fig. 9).

3.4.2. *Carbon Family*

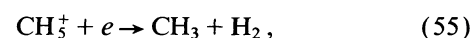
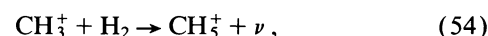
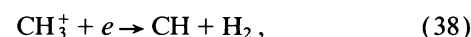
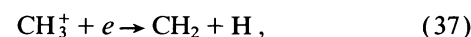
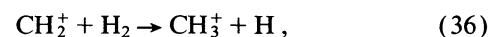
Most of the carbon is present in CO molecules in the dark core. The carbon chemistry is driven by the reactions



which are followed by radiative association

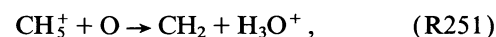


and the sequence



The initiating reaction (R222) is an additional source of atomic oxygen in the dark core.

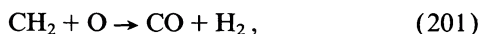
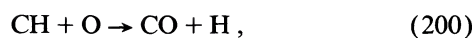
The electron density is small and the production of CH_2 , CH_3 , and CH_4 by reactions (R37), (R55), and (R56) is augmented by the reactions



and



The CH, CH_2 , and CH_3 molecules are removed by



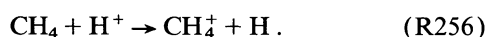
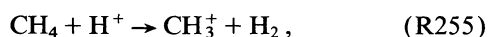
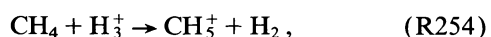
and by



The CH_4 molecules are removed by cosmic-ray-induced photodissociation



which is an additional source of CH_2 , as well as by



The dominant source of atomic carbon in the dark region is cosmic-ray-induced photodissociation of carbon monoxide



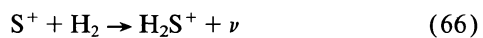
The carbon atoms are removed by



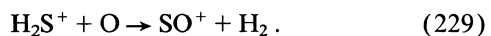
The CH_4 density becomes large in the dark core. The densities of the other species of the carbon family remain small (see Figs. 11, 12, and 13).

3.4.3. Sulfur Family

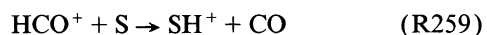
In the dark core most of the sulfur is driven into SO_2 molecules, and H_2S^+ ions are inefficiently produced by the reactions



and are rapidly removed by the pair of reactions



SH^+ ions are inefficiently produced by



and rapidly removed by



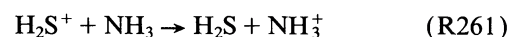
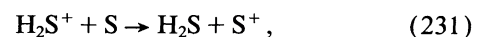
The sulfur atoms are supplied by the dissociative recombination



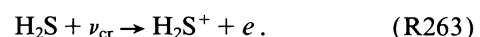
and are removed by



H_2S is inefficiently formed by



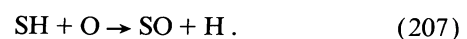
and is removed by cosmic-ray-induced photodissociation and photoionization



SH is formed by



and is removed by



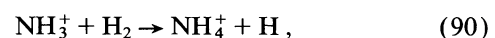
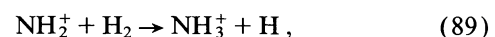
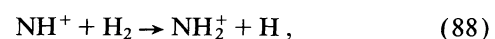
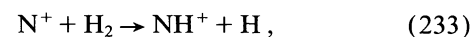
The densities of SH^+ , H_2S^+ , SH , and H_2S become very small in the dark core (see Fig. 15).

3.4.4. Nitrogen Family

Most of the nitrogen is molecular in the dark core, and the nitrogen chemistry is initiated by the reaction



which drives the sequence



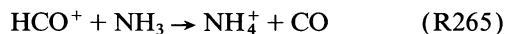
The NH_2 molecules produced in this sequence are removed by



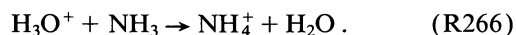
which is the dominant source of NH. The NH molecules are removed by



NH₃ is produced by reaction (R91) and is removed by

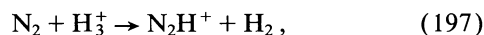


and

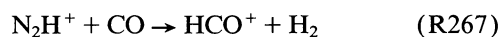


The NH₃ density becomes large in the dark core (see Fig. 21).

N₂H⁺ ions are produced by



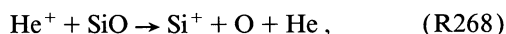
and, because the electron density is low, they are removed by the reaction



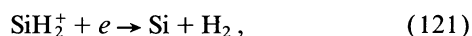
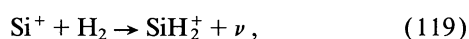
rather than by dissociative recombination in the dark core.

3.4.5. Silicon Family

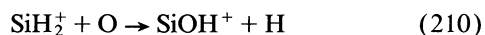
Most of the silicon is present in SiO molecules in the dark core. Si⁺ ions are produced by the reactions



which are followed by the sequence



The SiH₂⁺ ions are preferentially removed by



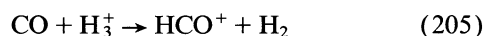
in the dark core, and the formation of SiH by reaction (R122) becomes inefficient. The SiH molecules are rapidly removed by



and the density of SiH becomes very small (see Fig. 18).

3.4.6. Oxygen Intermediates

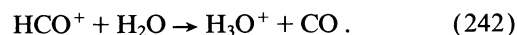
HCO⁺ is formed by



and is removed by



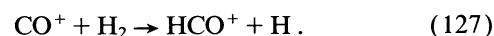
and by



CO⁺ ions are very inefficiently produced by



and are rapidly removed by



The HCO⁺ density becomes large in the dark core, while the CO⁺ density remains negligible (see Fig. 11).

SO⁺ ions are produced by



and by



and is removed by



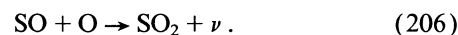
and the SO⁺ density becomes large in the dark core. SO is produced by cosmic-ray-induced photodissociation



which is an important source of atomic oxygen, and by



and is removed by



The SO₂ density becomes large, and the SO/SO₂ density ratio becomes small in the dark core (see Fig. 14).

NO is produced by reaction (R232) followed by



and is removed by



which is the main source of N₂ in the dark core. NO⁺ is produced by

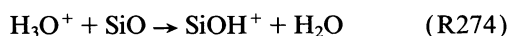


and is removed by



The NO^+ density and the NO^+/NO density ratio become large in the dark core (see Figs. 19 and 21).

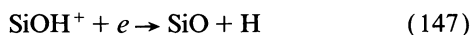
The SiO molecules are removed by



and by cosmic-ray-induced photodissociation



Reactions (R273) and (R274) are followed by



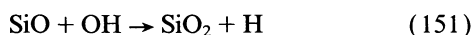
and



which is the main source of atomic silicon in the dark core. The atomic silicon is removed by



which is the dominant source of SiO in the dark core. SiO_2 is formed by



and is removed slowly by cosmic-ray-induced photodissociation



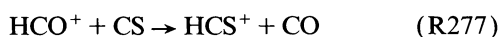
A larger SiO_2 density is maintained in the dark core than in the outer cloud layers (see Fig. 17).

3.4.7. Carbon Intermediates

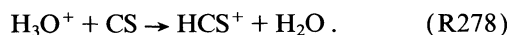
CS continues to be formed by



and is removed by



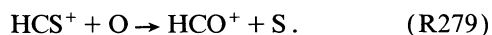
and



The CS density is about 10^{-3} times smaller in the dark core than at the edge of the S I zone (see Fig. 16). The HCS^+ ions produced by reactions (R277) and (R278) are removed by



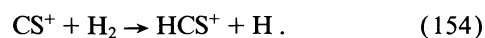
and



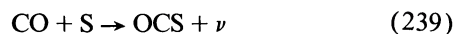
CS^+ ions are very inefficiently produced by



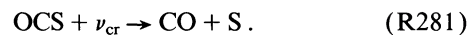
and are rapidly removed by



OCS is formed by



and removed by



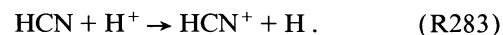
HCN is produced by



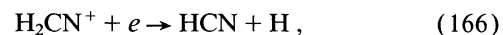
and is removed by



and by



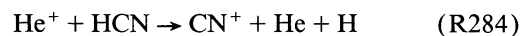
Reaction (R283) is followed by the sequence



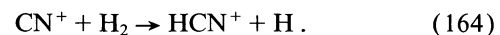
CN is produced by reactions (R167) and (R282) and is removed by



CN^+ is produced by



and is removed by



The CN^+/CN density ratio becomes large, and the HCN/CN density ratio remains large in the dark core (see Fig. 22).

4. SUMMARY

We have presented a detailed computation of the chemical structure of a photon-dominated region produced in a dense molecular exposed to an intense FUV radiation field. We have used our model in order to illustrate the gas-phase chemical processes that lead to the formation of atomic and molecular species at different depths through the cloud. Our results are

TABLE 2
ATOMIC AND MOLECULAR SPECIES IN DENSE PDRS^a

Family	Hot H I H/H ₂ <i>A_V</i> = 0 → 0.7	C II 0.7 → 1.7	S II 1.7 → 3.7	Si II 3.7 → 6	S I 3.7 → 7.6	Dark Core <i>A_V</i> > 10
Hydrogen	H H ⁺ H ₂ ⁺ H ₂ ⁺ H ₃ ⁺	H ₂ H ₂ ⁺	H ₂	H ₂	H ₂	H ₂ H ₃ ⁺
Oxygen	O O ⁺ OH H ₂ O OH ⁺ H ₂ O ⁺ H ₃ O ⁺ O ₂ O ₂ ⁺	O OH	O	O	O	O H ₂ O H ₃ O ⁺ O ₂ O ₂ ⁺
Carbon	C C ⁺ CH CH ₂ CH ₃ CH ⁺ CH ₂ ⁺ CH ₃ ⁺ CH ₄ ⁺ CH ₅ ⁺	C C ⁺ CH CH ₂ CH ₃ CH ⁺ CH ₂ ⁺ CH ₃ ⁺ CH ₄ ⁺ CH ₅ ⁺	CH ₄ CH ₅ ⁺
Sulfur	S ⁺ SH ⁺	S ⁺	S ⁺ SH H ₂ S ⁺	S	S H ₂ S H ₂ S ⁺	...
Nitrogen	N NH NH ₂ NH ⁺ NH ₂ ⁺ NH ₃ ⁺	N	N	N	N N ⁺ N ₂	N N ⁺ NH ₂ NH ₃ NH ₄ ⁺ N ₂ N ₂ H ⁺
Silicon	Si ⁺	Si ⁺	Si ⁺	Si Si ⁺ SiH SiH ₂ ⁺	Si Si ⁺	...
Oxygen intermediates	CO CO ⁺ HCO ⁺ SO ⁺ No NO ⁺ SiO ⁺ SiOH ⁺	CO ⁺ HCO ⁺	CO	CO	CO SO	CO HCO ⁺ SO SO ₂ SO ⁺ NO NO ⁺ SiOH ⁺ SiO SiO ₂
Carbon intermediates	CS ⁺ HCS ⁺ CN HCN CN ⁺ HCN ⁺ H ₂ CN ⁺	CS ⁺ HCS ⁺ CN HCN CN ⁺ HCN ⁺	CS HCS HCS ⁺ HCN OCS	HCS ⁺ HCN OCS

^a This table lists the atomic and molecular species that are preferentially produced in the different chemical zones present in a photon-dominated region with a total hydrogen particle density $n_T = 10^6 \text{ cm}^{-3}$, which is exposed to a FUV radiation field with $\chi = 2 \times 10^5$, and a cosmic-ray ionization rate of $\zeta = 5 \times 10^{-17} \text{ s}^{-1}$. The total elemental abundances are listed in Table 1.

summarized in Table 2 which lists the species that are preferentially produced in different chemical zones through the cloud. We identify these zones (in order of cloud depth) as a hot H I and H/H₂ transition layer, cold C II, S II, Si II, and S I zones, and a dark core. The locations of these zones in our model cloud are given in Table 2.

In the hot H I zone and H/H₂ transition layer the hydrogen is atomic, the carbon, sulfur, and silicon are singly ionized, and the oxygen and nitrogen are atomic. The molecules OH, CH⁺, NH, and SH⁺ are rapidly produced in the hot gas, and their densities become very large in the warm part of the H/H₂ transition layer. The large OH density leads to the efficient production of H⁺, OH⁺, H₂O⁺, H₃O⁺, H₃⁺, H₂O, O₂, O₂⁺, CO⁺, HCO⁺, CO, NO, NO⁺, SiO⁺, and SiOH⁺ in the hot gas. The large CH⁺ density leads to the efficient production of CH₂⁺, CH₃⁺, C, CH, CH₂, CS⁺, and HCS⁺, and the large CH⁺ and NH densities together lead to the efficient production of CN⁺, HCN⁺, CN, and HCN.

In the C II and S II zones sulfur and silicon are singly ionized, oxygen and nitrogen are atomic, and the hydrogen is fully molecular. The carbon is singly ionized in the C II zone, but is neutral (and present primarily in CO molecules) in the S II zone. The gas is cold in these cloud layers and molecule formation is less rapid than in the hot H I zone. The large C⁺ density in the C II zone leads to the efficient formation of C, CH⁺, CH₂⁺, CH₃⁺, CH, CH₂, CS⁺, HCS⁺, CN⁺, HCN⁺, CN, and HCN. Beyond the edge of the C II zone the C⁺ density becomes

small, and the densities of all of these species (with the exception of HCN) also become small. The CN/HCN density ratio is large in the C II zone and decreases at larger cloud depths. Evidence of enhanced CO⁺ densities and large CN/HCN density ratios in FUV-illuminated clouds has been presented by Latter et al. (1993), Störzer, Stutzki, & Sternberg (1995), and by Fuente et al. (1993). The sulfur hydrides SH and H₂S⁺ are efficiently produced in the S II zone where the S⁺ density remains large.

In the Si II and S I zones (which partially overlap) the carbon is locked in CO molecules, and the sulfur, oxygen, and nitrogen are atomic, and the hydrogen is molecular. The silicon is ionized in the Si II zone and is atomic in the S I zone. The silicon hydrides SiH and SiH₂⁺ are efficiently produced in the Si II zone where the Si⁺ density is large. The molecules and molecular ions H₂S, H₂S⁺, SO, CS, HCS, and HCS⁺ are efficiently produced in the S I zone. The densities of H₂S and CS are much larger near the inner edge of the S I zone than at deeper cloud depths. The CS molecule may be a tracer of FUV-illuminated clouds in addition to being a tracer of dense molecular gas. Evidence for photochemically enhanced CS and H₂S abundances in FUV-illuminated clouds has been presented by Zhou et al. (1991) and Jansen et al. (1994).

At sufficiently large cloud depths a dark core exists in which the chemistry is dominated by cosmic-ray ionization and the incident FUV photons no longer influence the molecular formation and destruction. The gas-phase carbon, sulfur, nitro-

TABLE 3
SELECTED MOLECULAR DIAGNOSTICS^a

Density Ratio	Hot H I H/H ₂ $A_V = 0.6$	C II $A_V = 1.5$	S II $A_V = 3$	Si II $A_V = 5$	S I $A_V = 7$	Dark Core $A_V > 10$
OH/H ₂ O	4.5 (1) ^b	2.3 (1)	9.3	9.2 (-2)	4.4 (-3)	3.4 (-4)
OH ⁺ /H ₃ O ⁺	1.8	1.3	7.5 (-2)	9.6 (-3)	1.3 (-3)	1.4 (-5)
CO ⁺ /HCO ⁺	5.1 (-2)	3.5 (-2)	1.5 (-4)	1.7 (-6)	2.9 (-7)	2.0 (-7)
SO ⁺ /SO	1.7	2.3 (-1)	2.8 (-3)	6.4 (-4)	1.2 (-4)	5.7 (-4)
SiO ⁺ /SiO	1.6 (-1)	5.7 (-3)	3.0 (-5)	1.2 (-7)	1.8 (-9)	1.7 (-10)
NH/NH ₃	7.8 (4)	2.2 (5)	9.2 (3)	9.3 (-1)	1.7 (-2)	4.9 (-4)
CN/HCN	4.7	1.1 (1)	8.4	3.3 (-1)	1.3 (-3)	1.8 (-4)

^a Selected molecular density ratios at specific locations in the different chemical zones present in a photon-dominated region with a total hydrogen particle density $n_T = 10^6 \text{ cm}^{-3}$, which is exposed to a FUV radiation field with $\chi = 2 \times 10^5$, and a cosmic-ray ionization rate of $\zeta = 5 \times 10^{-17} \text{ s}^{-1}$. The total elemental abundances are listed in Table 1.

^b Numbers in parentheses are exponents. For example, 4.5 (1) = 4×10^1 .

gen, and silicon are present in CO, SO₂, N₂, and SiO₂ molecules respectively. The excess oxygen not driven into CO remains primarily in atomic form. In our model most of the positive charge is carried by molecular ions which recombine rapidly and the fractional ionization becomes small in the dark core. The densities of the saturated molecules and molecular ions H₃O⁺, H₂O, O₂, O₂⁺, HCO⁺, NH₄⁺, NH₃, N₂H⁺, SO⁺, SO₂, NO⁺, NO, SiOH⁺, SiO, HCS⁺, HCN, and OCS become large in the dark core.

In Table 3 we list a set of specific molecular density ratios which may be used as diagnostics of the different chemical zones in the cloud. This table shows that the OH/H₂O, OH⁺/H₃O⁺, CO⁺/HCO⁺, SO⁺/SO, SiO⁺/SiO, NH/NH₃, and CN/HCN density ratios are largest in the outer chemical zones. Very large SO⁺/SO and SiO⁺/SiO density ratios are produced in the hot H I zone and H/H₂ transition layer. The OH⁺/H₃O⁺, CO⁺/HCO⁺, and NH/NH₃ ratios remain large through the C II zone, and the OH/H₂O, and CN/HCN ratios remain large through the S II zone. All of these density ratios become very small at large cloud depths.

The fractional ionization is controlled by the sequential photoionization of carbon, sulfur, and silicon through the PDR, and by cosmic-ray ionization of hydrogen and helium in the dark core. The fractional ionization ranges from 3×10^{-4} near the cloud surface to 3×10^{-9} in the dark core (see Fig. 8).

The ambipolar diffusion rates, and the magnetically regulated cloud collapse times (Shu, Adams, & Lizano 1987; McKee 1989), are therefore sensitive to the cloud depth and to the molecular abundances and density ratios (such as those listed in Table 3) in the different chemical zones.

We have demonstrated that the abundances of many molecular species may be significantly enhanced in the photon-dominated regions of molecular clouds, and that specific molecular density ratios exist which may be used as diagnostics of photo-driven chemistry. However, our model is illustrative. The locations and sizes of the various chemical zones, and the abundances of the atomic and molecular species are, in general, sensitive to the total hydrogen gas density, the intensity of the incident FUV radiation field, the grain absorption and scattering properties, the total elemental abundances, and the cosmic-ray ionization rate. We will present a parameter study elsewhere.

We thank W. G. Roberge for providing us with his radiative transfer program, and D. Jones for his assistance in using it. We thank E. F. van Dishoeck, R. Genzel, A. I. Harris, D. T. Jaffe, H. Störzer, and J. Stutzki for useful discussions. This work has been partly supported by the Smithsonian Astrophysical Observatory and partly by the National Science Foundation through grant AST-93-01009.

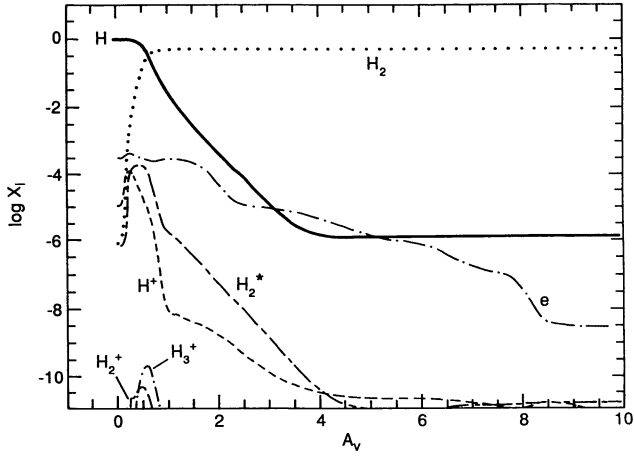


FIG. 8a

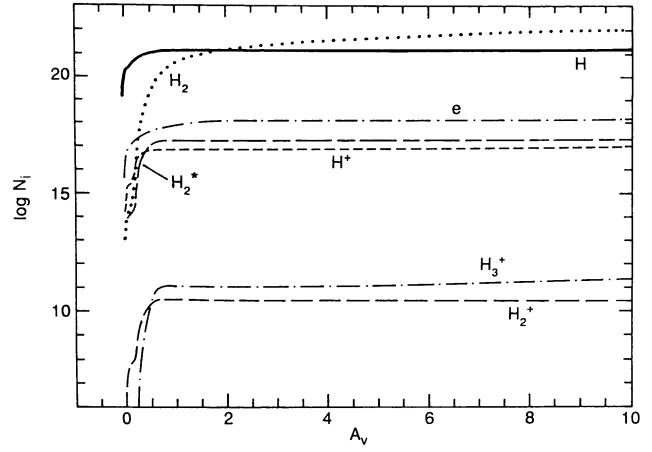


FIG. 8b

FIG. 8.—(a) Abundances $x_i \equiv n_i/n$ (where n is the density of hydrogen nuclei and n_i are the densities of species i) of H, H₂, H₂⁺, H⁺, H₂⁺, H₃⁺, and e . (b) Integrated column densities N_i (cm⁻²) of H, H₂, H₂⁺, H⁺, H₂⁺, H₃⁺, and e .

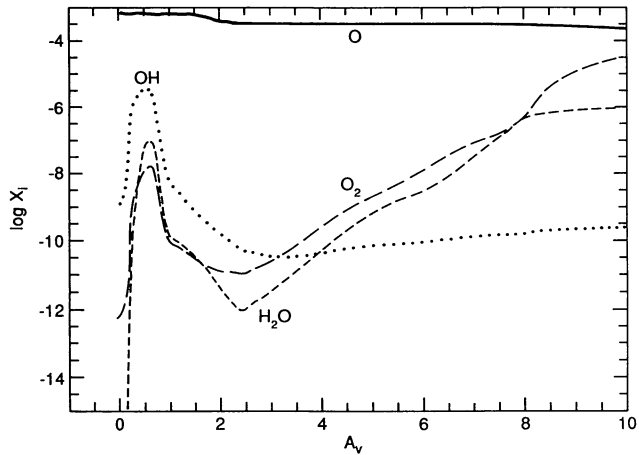


FIG. 9a

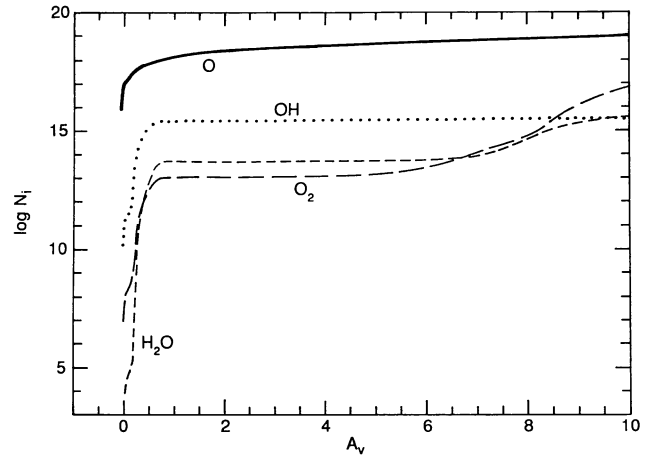


FIG. 9b

FIG. 9.—(a) Abundances of O, OH, H₂O, and O₂. (b) Column densities of O, OH, H₂O, and O₂.

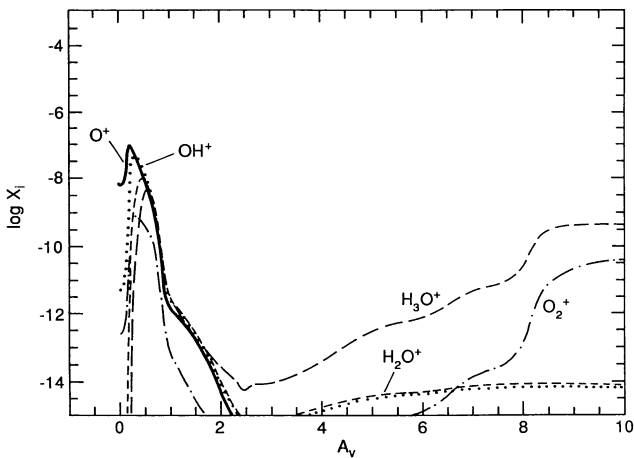


FIG. 10a

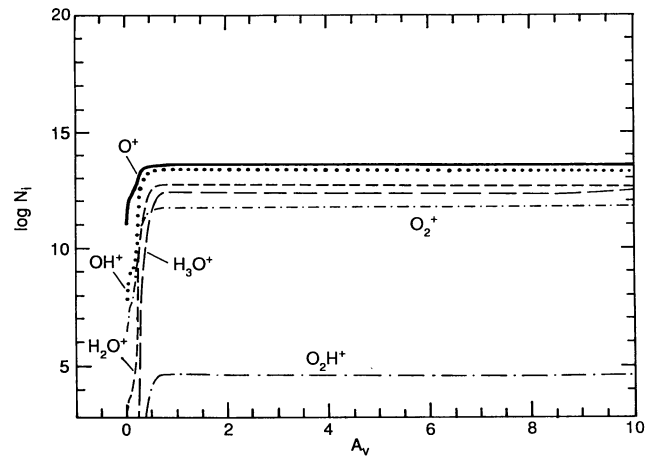


FIG. 10b

FIG. 10.—(a) Abundances of O⁺, OH⁺, H₂O⁺, H₃O⁺, and O₂⁺. (b) Column densities of O⁺, OH⁺, H₂O⁺, H₃O⁺, and O₂⁺.

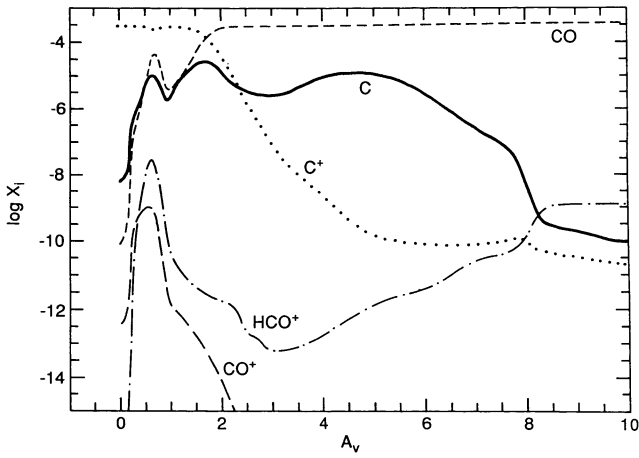


FIG. 11a

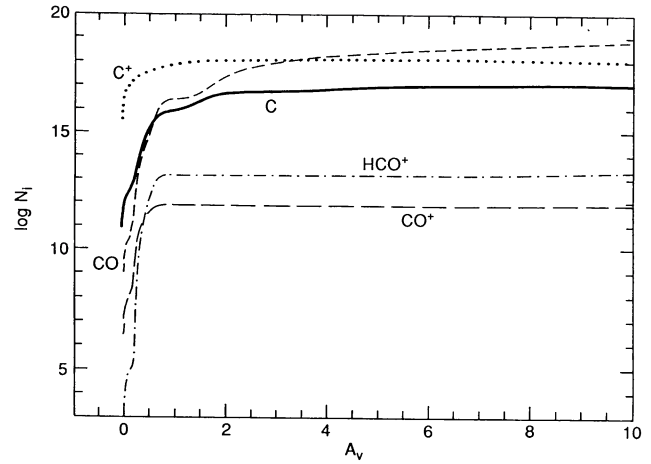


FIG. 11b

FIG. 11.—(a) Abundances of C, C⁺, CO, CO⁺, and HCO⁺. (b) Column densities of C, C⁺, CO, CO⁺, and HCO⁺.

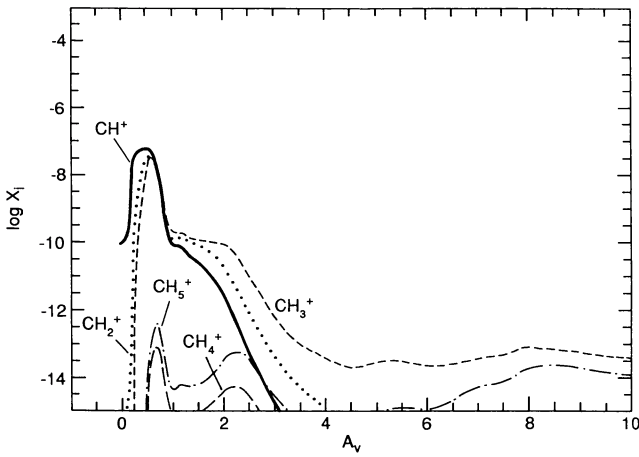


FIG. 12a

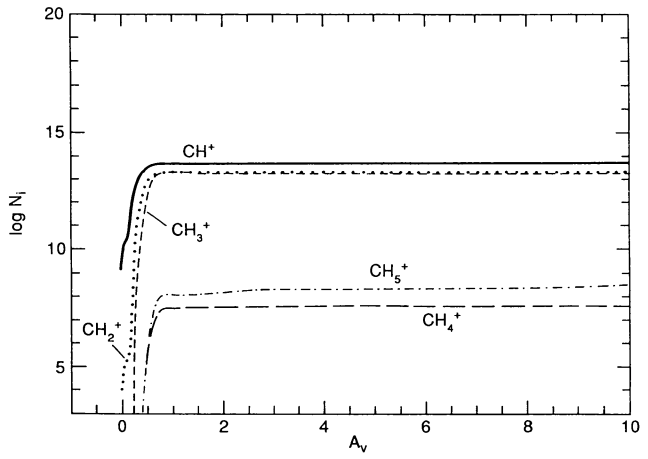


FIG. 12b

FIG. 12.—(a) Abundances of CH⁺, CH₂⁺, CH₃⁺, CH₄⁺, and CH₅⁺. (b) Column densities of CH⁺, CH₂⁺, CH₃⁺, CH₄⁺, and CH₅⁺.

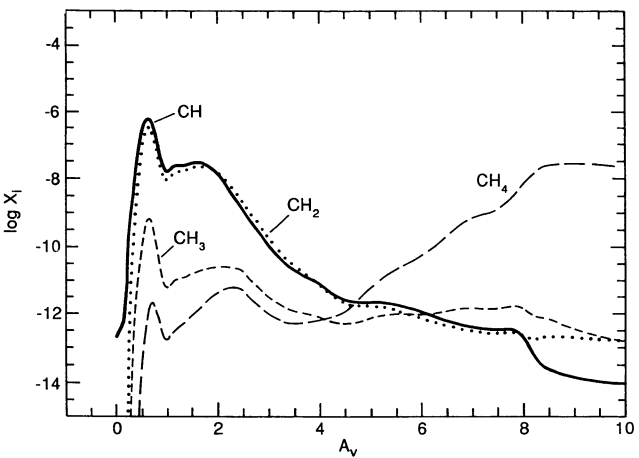


FIG. 13a

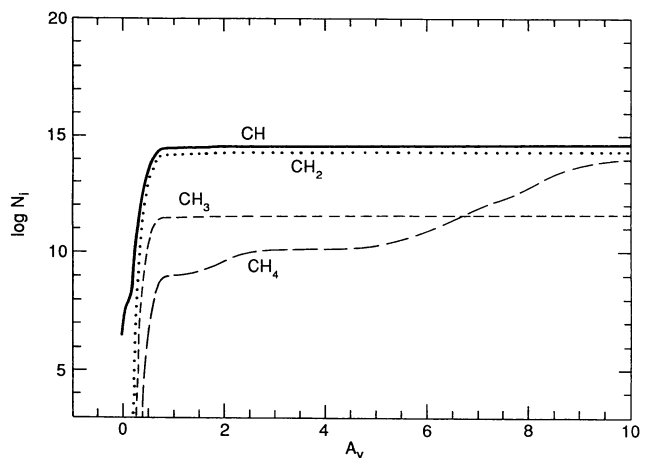


FIG. 13b

FIG. 13.—(a) Abundances of CH, CH₂, CH₃, and CH₄. (b) Column densities of CH, CH₂, CH₃, and CH₄.

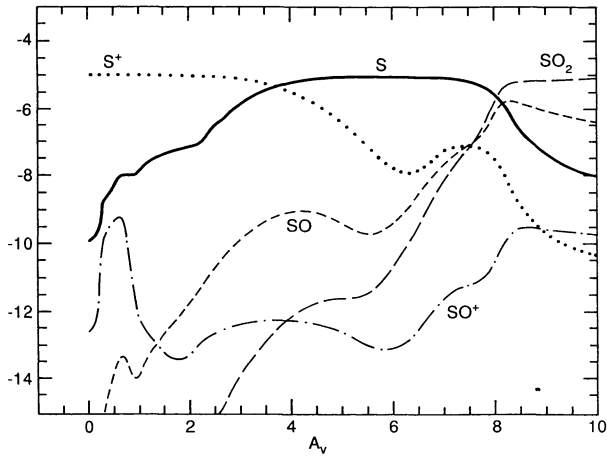


FIG. 14a

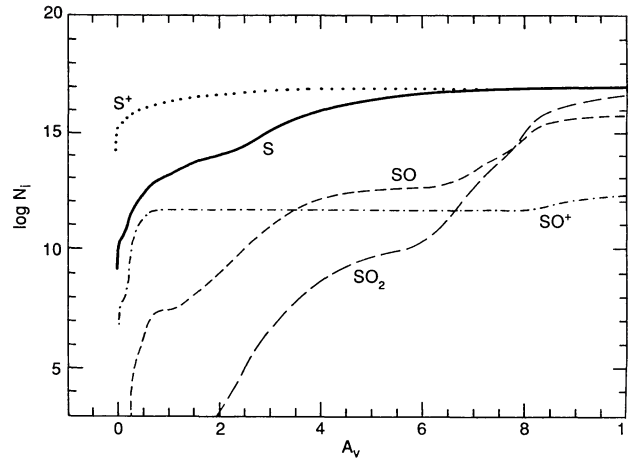


FIG. 14b

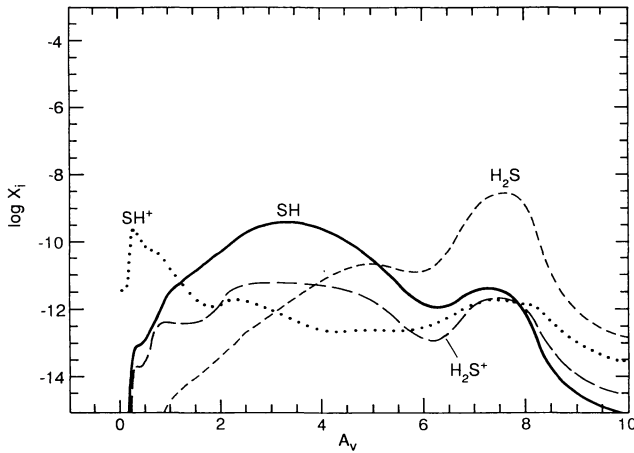
FIG. 14.—(a) Abundances of S^+ , S , SO , and SO_2 , and SO^+ . (b) Column densities of S^+ , S , SO , SO_2 , and SO^+ .

FIG. 15a

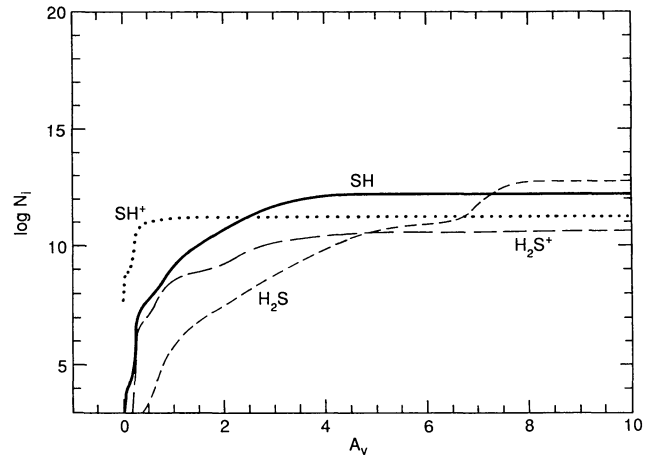


FIG. 15b

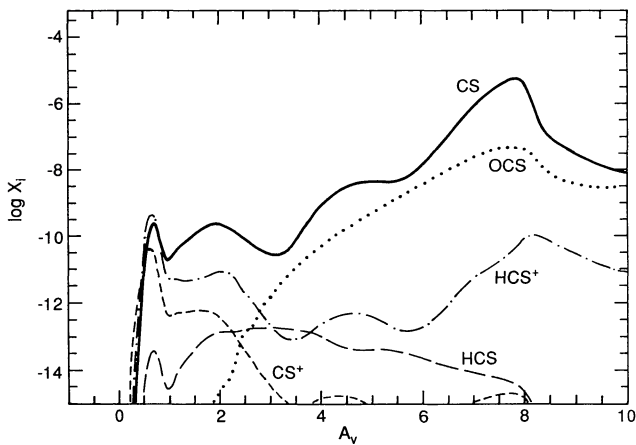
FIG. 15.—(a) Abundances of SH , H_2S , SH^+ , and H_2S^+ . (b) Column densities of SH , H_2S , SH^+ , and H_2S^+ .

FIG. 16a

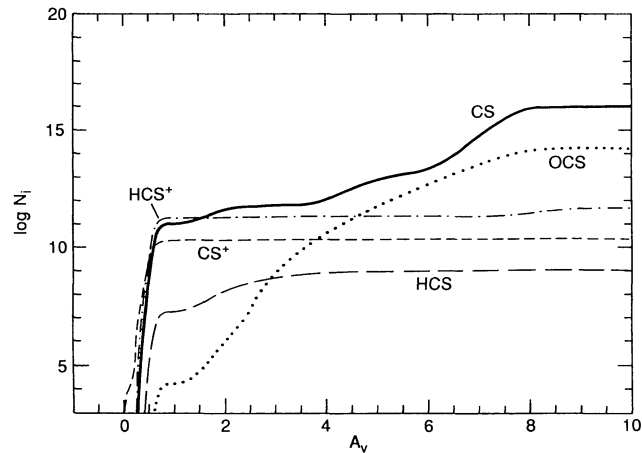


FIG. 16b

FIG. 16.—(a) Abundances of CS , HCS , OCS , CS^+ , and HCS^+ . (b) Column densities of CS , HCS , OCS , CS^+ , and HCS^+ .

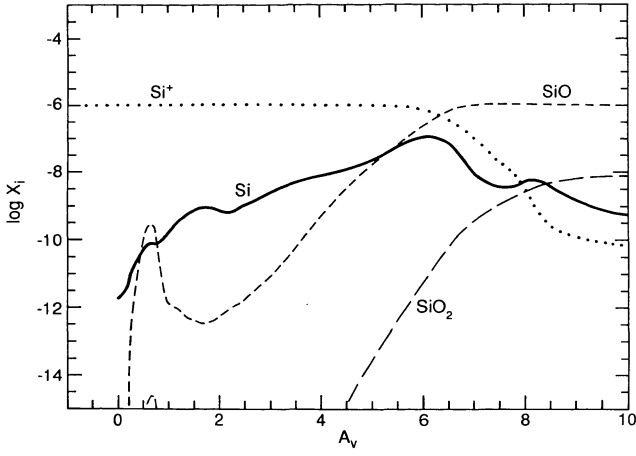


FIG. 17a

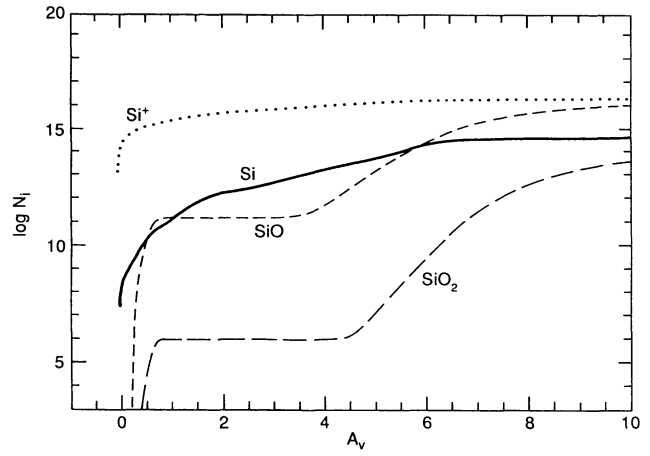


FIG. 17b

FIG. 17.—(a) Abundances of Si, Si⁺, SiO, and SiO₂. (b) Column densities of Si, Si⁺, SiO, and SiO₂.

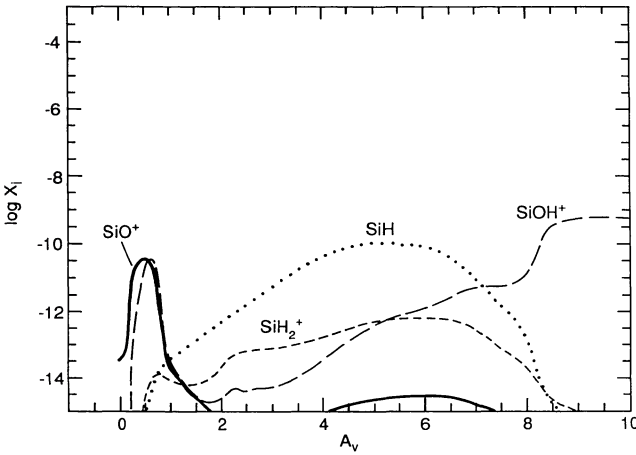


FIG. 18a

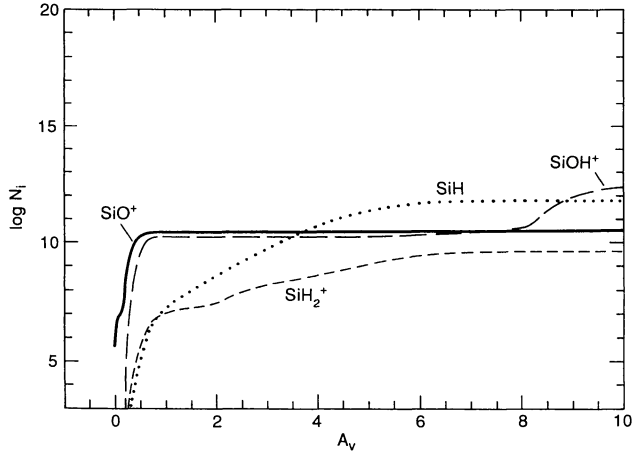


FIG. 18b

FIG. 18.—(a) Abundances of SiH, SiH₂⁺, SiO⁺, and SiOH⁺. (b) Column densities of SiH, SiH₂⁺, SiO⁺, and SiOH⁺.

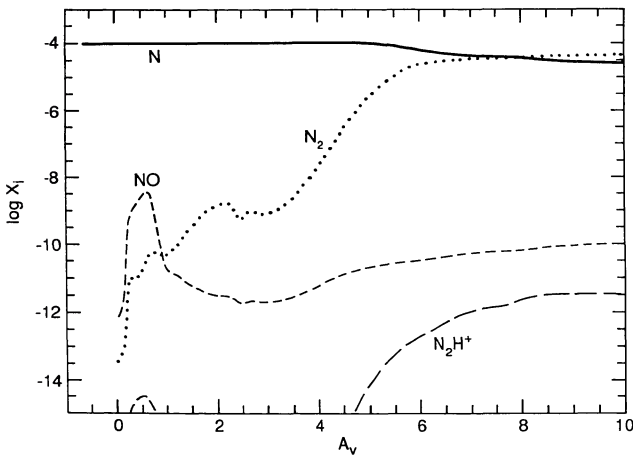


FIG. 19a

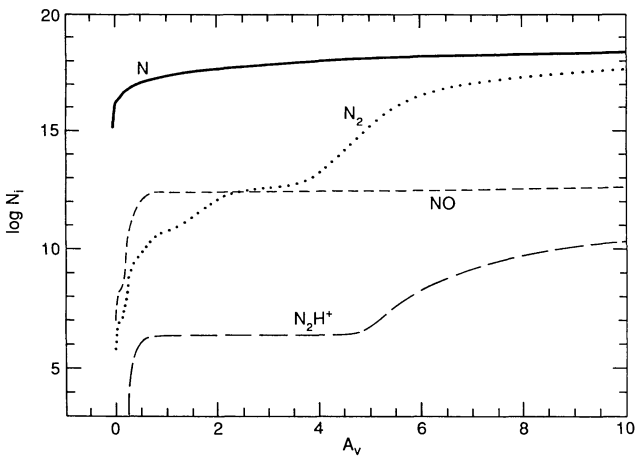


FIG. 19b

FIG. 19.—(a) Abundances of N, N₂, NO, and N₂H⁺. (b) Column densities of N, N₂, NO, and N₂H⁺.

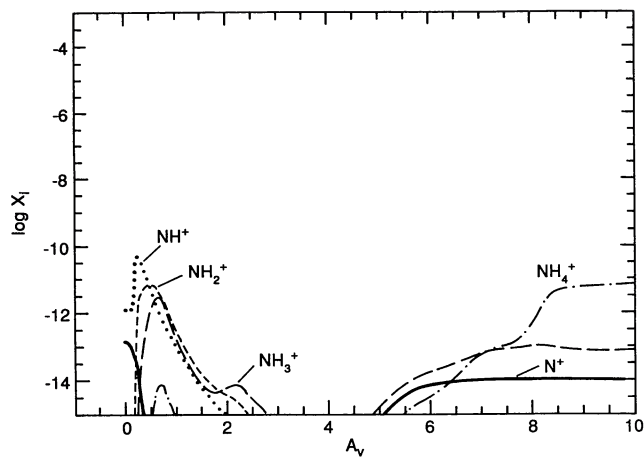


FIG. 20a

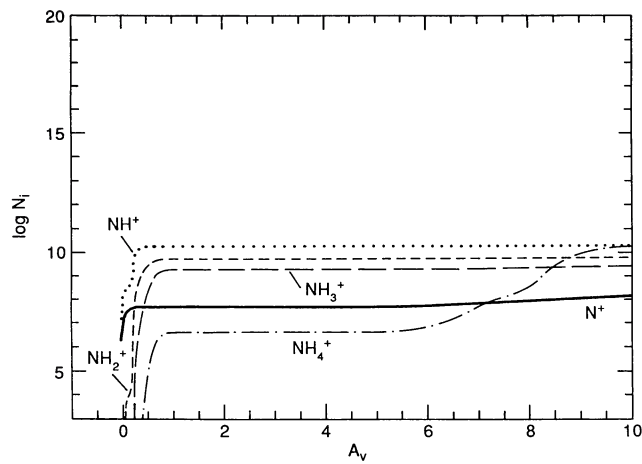


FIG. 20b

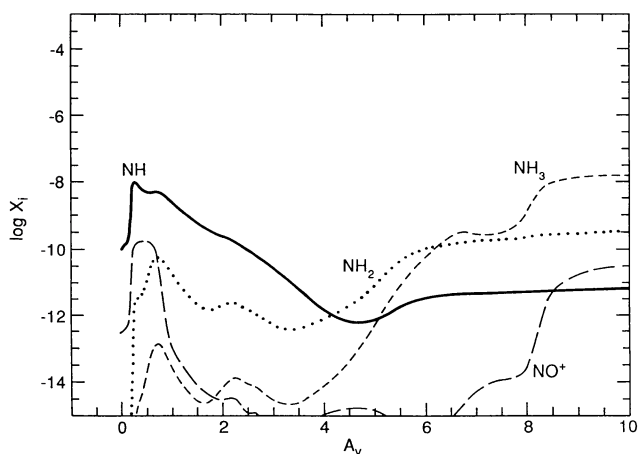
FIG. 20.—(a) Abundances of N^+ , NH^+ , NH_2^+ , NH_3^+ , and NH_4^+ . (b) Column densities of N^+ , NH^+ , NH_2^+ , NH_3^+ , and NH_4^+ .

FIG. 21a

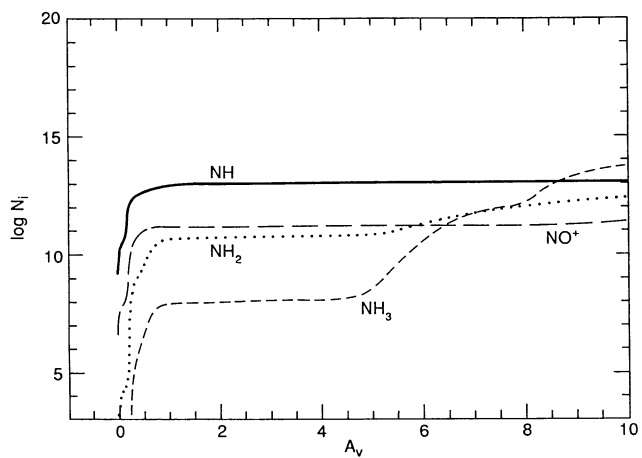


FIG. 21b

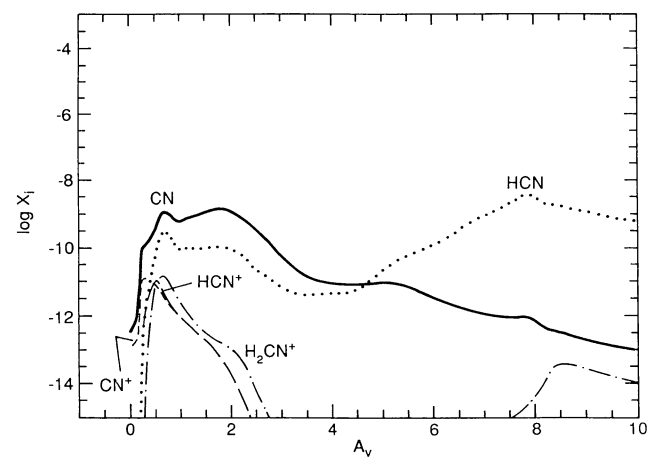
FIG. 21.—(a) Abundances of NH , NH_2 , NH_3 , and NO^+ . (b) Column densities of NH , NH_2 , NH_3 , and NO^+ .

FIG. 22a

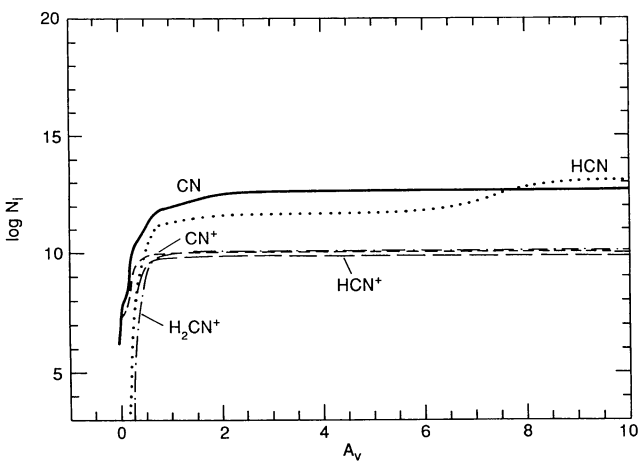


FIG. 22b

FIG. 22.—(a) Abundances of CN , HCN , CN^+ , HCN^+ , and H_2CN^+ . (b) Column densities of CN , HCN , CN^+ , HCN^+ , and H_2CN^+ .

In this appendix we describe some of the basic input data and approximations that we employed in carrying out our calculations.

A1. CHEMISTRY

A1.1. Photoionization and Photodissociation Rates

In our model we assume that a semi-infinite plane-parallel cloud is exposed to an isotropic far-ultraviolet radiation field given by Draine's (1978) fit to the specific photon intensity of the average interstellar FUV field

$$I(\nu) = \frac{1}{4\pi} \left(\frac{1.068 \times 10^{-4}}{\lambda} - \frac{1.719 \times 10^{-2}}{\lambda^2} + \frac{6.853 \times 10^{-1}}{\lambda^3} \right) \text{ photons cm}^{-2} \text{ s}^{-1} \text{ Hz}^{-1} \text{ sr}^{-1} \quad (\text{A1})$$

multiplied by an intensity scaling factor $\chi = 2 \times 10^5$.

As the FUV radiation penetrates the cloud it is scattered and absorbed by dust grains and the rates of atomic and molecular photoionization and photodissociation diminish. In our model we adopted the grain scattering and absorption properties calculated by Draine & Lee (1984) for a "Mathis-Rumpl-Nordsieck" mixture of graphite and silicate grains (Mathis, Rumpl, & Nordsieck 1977), and we used the analytic bi-exponential expressions

$$\Gamma_i = \chi C_i \exp(-\alpha_i A_V - \beta_i A_V^2) \text{ s}^{-1} \quad (\text{A2})$$

presented by Roberge et al. (1991) for the resulting depth-dependent photoionization and photodissociation rates. In these expressions A_V is the visual extinction measured from the cloud surface, and C_i , α_i and β_i are attenuation parameters that depend on the atomic or molecular FUV photo-absorption cross sections, the grain properties, and the total cloud thickness A_V^{tot} . In our calculations we adopted attenuation parameters appropriate for optically thick clouds with $A_V^{\text{tot}} = 100$. We assume a gas-to-dust mass ratio such that $A_V = 4.75 \times 10^{-22} N$ where N is the total column density (cm^{-2}) of hydrogen nuclei from the cloud surface.

We used the "spherical harmonics" radiative transfer program and fitting procedures developed and described by Roberge et al. in order to compute the coefficients C_i , α_i and β_i (for $A_V^{\text{tot}} = 100$) for several species (C, Si, S, H₂, CO, N₂, and OH⁺) not considered by Roberge et al. but for which FUV absorption cross sections are available. In Table 4 we list the rates of atomic photoionization and molecular photodissociation for these species in an unattenuated Draine field. For species with unknown FUV absorption cross sections we set $\alpha = 2.55$ and $\beta = -1.65 \times 10^{-2}$ which we computed using the Roberge et al. program assuming wavelength-independent cross sections. In Table 5 we list the values of C_i , α_i , and β_i that we used for each of the photoreactions included in our calculations.

The photodissociation rates of H₂ and CO are also diminished by "self-shielding" as the FUV absorption lines through which these molecules dissociate become optically thick (Federman, Glassgold, & Kwan 1979; Sternberg 1988; van Dishoeck & Black 1988; Abgrall et al. 1992). In our calculations we assumed that the FUV line and continuum attenuation are separable (Sternberg & Dalgarno 1989), and that the depth-dependent H₂ photodissociation rate is given by

$$\dot{\Gamma}_{\text{H}_2} = \chi \frac{\pi e^2}{mc} \left[\sum_{\nu} I_{\nu}(\nu) f_{\nu} \eta_{\nu} g_{\nu}(N_{\text{H}_2}) \right] e^{-\alpha_{\text{H}_2} A_V - \beta_{\text{H}_2} A_V^2} \text{ s}^{-1}. \quad (\text{A3})$$

TABLE 4
PHOTOREACTION RATES^a

Photoreaction	s ⁻¹
H ₂ + ν → H + H	4.9 (-11)
C + ν → C ⁺ + e	2.4 (-10)
S + ν → S ⁺ + e	4.3 (-10)
N ₂ + ν → N + N	2.1 (-10)
Si + ν → Si ⁺ + e	3.1 (-9)
CO + ν → C + O	2.0 (-10)
OH ⁺ + ν → H ⁺ + O	1.2 (-11)

^a This table lists the rates of molecular photodissociation and atomic photoionization in an unattenuated Draine field for several species not included in the compilation of Roberge et al. 1991 for which FUV photoabsorption cross section data are available. See Table 5 for references.

TABLE 5
PHOTOREACTION ATTENUATION PARAMETERS

Photoreaction	C	α	β	Reference
$H_2 + \nu \rightarrow H + H$	1.33 (-11)	3.78	-1.04 (-2)	3
$OH + \nu \rightarrow O + H$	9.35 (-11)	2.13	-1.66 (-2)	2
$H_2O + \nu \rightarrow O + H_2$	1.00 (-11)	2.55	-1.65 (-2)	1
$H_2O + \nu \rightarrow OH + H$	1.62 (-10)	2.10	-1.63 (-2)	2
$H_2O + \nu \rightarrow H_2O^+ + e$	5.00 (-12)	2.55	-1.65 (-2)	1
$O_2 + \nu \rightarrow O + O$	2.32 (-10)	2.23	-1.54 (-2)	2
$O_2 + \nu \rightarrow O_2^+ + e$	1.82 (-11)	3.83	-9.95 (-3)	2
$C + \nu \rightarrow C^+ + e$	7.45 (-11)	3.51	-1.58 (-2)	4
$CH + \nu \rightarrow C + H$	2.43 (-10)	1.74	-2.21 (-2)	2
$CH + \nu \rightarrow CH^+ + e$	1.50 (-10)	2.55	-1.65 (-2)	1
$CH_2 + \nu \rightarrow CH + H$	2.50 (-11)	2.55	-1.65 (-2)	1
$CH_2 + \nu \rightarrow CH_2^+ + e$	2.50 (-10)	2.55	-1.65 (-2)	1
$CH_3 + \nu \rightarrow CH + H_2$	2.50 (-11)	2.55	-1.65 (-2)	1
$CH_3 + \nu \rightarrow CH_2 + H$	2.50 (-11)	2.55	-1.65 (-2)	1
$CH_3 + \nu \rightarrow CH_3^+ + e$	1.50 (-10)	2.55	-1.65 (-2)	1
$CH_4 + \nu \rightarrow CH_2 + H_2$	2.94 (-10)	2.61	-2.03 (-2)	2
$CH_4 + \nu \rightarrow CH + H_2 + H$	1.00 (-10)	2.55	-1.65 (-2)	1
$CH_4 + \nu \rightarrow CH_3 + H$	1.00 (-10)	2.55	-1.65 (-2)	1
$CH_4 + \nu \rightarrow CH_4^+ + e$	1.50 (-10)	2.55	-1.65 (-2)	1
$S + \nu \rightarrow S^+ + e$	1.22 (-10)	3.13	-1.61 (-2)	5
$SH + \nu \rightarrow S + H$	5.00 (-10)	2.55	-1.65 (-2)	1
$SH + \nu \rightarrow SH^+ + e$	3.00 (-10)	2.55	-1.65 (-2)	1
$H_2S + \nu \rightarrow SH + H$	7.32 (-10)	2.38	-2.61 (-2)	2
$H_2S + \nu \rightarrow H_2S^+ + e$	1.85 (-10)	3.30	-1.22 (-2)	2
$NH + \nu \rightarrow N + H$	1.68 (-10)	2.37	-1.62 (-2)	6
$NH + \nu \rightarrow NH^+ + e$	5.00 (-12)	2.55	-1.65 (-2)	1
$NH_2 + \nu \rightarrow NH + H$	1.46 (-11)	1.90	-6.20 (-3)	2
$NH_2 + \nu \rightarrow NH_2^+ + e$	7.50 (-11)	2.55	-1.65 (-2)	1
$NH_3 + \nu \rightarrow NH_2 + H$	3.05 (-10)	2.16	-1.71 (-2)	2
$NH_3 + \nu \rightarrow NH_3^+ + e$	5.27 (-11)	3.35	-1.58 (-2)	2
$N_2 + \nu \rightarrow N + N$	6.76 (-11)	3.86	-7.71 (-3)	7
$Si + \nu \rightarrow Si^+ + e$	9.65 (-10)	2.37	-1.47 (-2)	8
$SiH + \nu \rightarrow Si + H$	1.50 (-9)	2.55	-1.65 (-2)	1
$SiO + \nu \rightarrow Si + O$	5.00 (-11)	2.55	-1.65 (-2)	1
$SiO + \nu \rightarrow SiO^+ + e$	5.00 (-11)	2.55	-1.65 (-2)	1
$SiO_2 + \nu \rightarrow SiO + O$	2.00 (-10)	2.55	-1.65 (-2)	1
$CO + \nu \rightarrow C + O$	3.53 (-11)	3.47	-1.31 (-2)	9
$SO + \nu \rightarrow O + S$	2.00 (-9)	2.55	-1.65 (-2)	1
$SO + \nu \rightarrow SO^+ + e$	3.00 (-10)	2.55	-1.65 (-2)	1
$SO_2 + \nu \rightarrow SO + O$	5.17 (-10)	2.30	-2.30 (-2)	2
$CS + \nu \rightarrow C + S$	5.00 (-10)	2.55	-1.65 (-2)	1
$CS + \nu \rightarrow CS^+ + e$	1.00 (-10)	2.55	-1.65 (-2)	1
$NO + \nu \rightarrow N + O$	1.31 (-10)	2.07	-1.40 (-2)	2
$NO + \nu \rightarrow NO^+ + e$	6.50 (-11)	2.55	-1.65 (-2)	1
$HCS + \nu \rightarrow CS + H$	2.00 (-10)	2.55	-1.65 (-2)	1
$CN + \nu \rightarrow C + N$	3.55 (-10)	3.71	-8.14 (-3)	2
$HCN + \nu \rightarrow CN + H$	3.44 (-10)	2.69	-3.73 (-2)	2
$OCS + \nu \rightarrow CO + S$	1.19 (-9)	2.05	-1.28 (-2)	2
$H_2^+ + \nu \rightarrow H^+ + H$	2.25 (-10)	2.55	-1.65 (-2)	1
$H_3^+ + \nu \rightarrow H^+ + H_2$	2.50 (-13)	2.55	-1.65 (-2)	1
$H_3^+ + \nu \rightarrow H_2^+ + H$	2.50 (-13)	2.55	-1.65 (-2)	1
$OH^+ + \nu \rightarrow H^+ + O$	2.04 (-12)	3.35	-8.16 (-2)	10
$H_2O^+ + \nu \rightarrow H_2^+ + O$	5.00 (-11)	2.55	-1.65 (-2)	1
$H_2H^+ + \nu \rightarrow H^+ + OH$	5.00 (-11)	2.55	-1.65 (-2)	1
$H_2O^+ + \nu \rightarrow O^+ + H_2$	5.00 (-11)	2.55	-1.65 (-2)	1
$H_2O^+ + \nu \rightarrow OH^+ + H$	1.50 (-10)	2.55	-1.65 (-2)	1
$H_3O^+ + \nu \rightarrow H^+ + H_2O$	2.50 (-11)	2.55	-1.65 (-2)	1
$H_3O^+ + \nu \rightarrow H_2^+ + OH$	2.50 (-11)	2.55	-1.65 (-2)	1
$H_3O^+ + \nu \rightarrow H_2O^+ + H$	7.50 (-12)	2.55	-1.65 (-2)	1
$H_3O^+ + \nu \rightarrow OH^+ + H_2$	2.50 (-11)	2.55	-1.65 (-2)	1
$O_2^+ + \nu \rightarrow O + O^+$	5.00 (-11)	2.55	-1.65 (-2)	1
$CH^+ + \nu \rightarrow H^+ + C$	8.12 (-11)	3.71	-2.05 (-2)	2
$CH_2^+ + \nu \rightarrow CH^+ + H$	2.50 (-10)	2.55	-1.65 (-2)	1
$CH_3^+ + \nu \rightarrow CH_2^+ + H$	2.50 (-10)	2.55	-1.65 (-2)	1
$CH_3^+ + \nu \rightarrow CH^+ + H_2$	2.50 (-10)	2.55	-1.65 (-2)	1
$CH_4^+ + \nu \rightarrow CH_2^+ + H_2$	2.50 (-10)	2.55	-1.65 (-2)	1
$CH_4^+ + \nu \rightarrow CH_3^+ + H$	2.50 (-10)	2.55	-1.65 (-2)	1
$CH_5^+ + \nu \rightarrow CH_4^+ + H$	2.50 (-10)	2.55	-1.65 (-2)	1
$CH_5^+ + \nu \rightarrow CH_3^+ + H_2$	2.50 (-10)	2.55	-1.65 (-2)	1

TABLE 5—Continued

Photoreaction	C	α	β	Reference
$\text{SH}^+ + \nu \rightarrow \text{S}^+ + \text{H}$	5.00 (–13)	2.55	–1.65 (–2)	1
$\text{H}_2\text{S}^+ + \nu \rightarrow \text{SH}^+ + \text{H}$	2.00 (–10)	2.55	–1.65 (–2)	1
$\text{NH}^+ + \nu \rightarrow \text{N} + \text{H}^+$	5.00 (–11)	2.55	–1.65 (–2)	1
$\text{NH}_2^+ + \nu \rightarrow \text{NH} + \text{H}^+$	2.50 (–10)	2.55	–1.65 (–2)	1
$\text{NH}_3^+ + \nu \rightarrow \text{NH} + \text{H}_2^+$	2.50 (–11)	2.55	–1.65 (–2)	1
$\text{NH}_3^+ + \nu \rightarrow \text{NH}_2 + \text{H}^+$	2.50 (–11)	2.55	–1.65 (–2)	1
$\text{NH}_3^+ + \nu \rightarrow \text{NH}^+ + \text{H}_2$	2.50 (–11)	2.55	–1.65 (–2)	1
$\text{NH}_3^+ + \nu \rightarrow \text{NH}_2^+ + \text{H}$	1.75 (–10)	2.55	–1.65 (–2)	1
$\text{NH}_4^+ + \nu \rightarrow \text{NH}_3^+ + \text{H}$	2.50 (–10)	2.55	–1.65 (–2)	1
$\text{NH}_4^+ + \nu \rightarrow \text{NH}_2^+ + \text{H}_2$	2.50 (–10)	2.55	–1.65 (–2)	1
$\text{N}_2\text{H}^+ + \nu \rightarrow \text{N}_2 + \text{H}^+$	5.00 (–11)	2.55	–1.65 (–2)	1
$\text{CO}^+ + \nu \rightarrow \text{C}^+ + \text{O}$	1.50 (–11)	2.55	–1.65 (–2)	1
$\text{HCO}^+ + \nu \rightarrow \text{CO}^+ + \text{H}$	1.50 (–10)	2.55	–1.65 (–2)	1
$\text{SO}^+ + \nu \rightarrow \text{S}^+ + \text{O}$	5.00 (–11)	2.55	–1.65 (–2)	1
$\text{SiO}^+ + \nu \rightarrow \text{Si}^+ + \text{O}$	1.50 (–11)	2.55	–1.65 (–2)	1
$\text{SiOH}^+ + \nu \rightarrow \text{SiO}^+ + \text{H}$	1.50 (–11)	2.55	–1.65 (–2)	1
$\text{CS}^+ + \nu \rightarrow \text{S}^+ + \text{C}$	1.00 (–10)	2.55	–1.65 (–2)	1
$\text{HCS}^+ + \nu \rightarrow \text{CS}^+ + \text{H}_2$	2.00 (–10)	2.55	–1.65 (–2)	1
$\text{CN}^+ + \nu \rightarrow \text{C}^+ + \text{N}$	5.00 (–11)	2.55	–1.65 (–2)	1
$\text{HCN}^+ + \nu \rightarrow \text{CN} + \text{H}^+$	5.00 (–11)	2.55	–1.65 (–2)	1
$\text{H}_2\text{CN}^+ + \nu \rightarrow \text{HCN} + \text{H}^+$	5.00 (–11)	2.55	–1.65 (–2)	1

^a The depth-dependent atomic and molecular photoionization and photodissociation rates are given by $G = \chi C \exp(-\alpha A_\nu - \beta A_\nu^2) \text{ s}^{-1}$. For $A_\nu > 15$ the parameters α and β should be replaced by $\alpha' = \alpha + 7.5 \times \beta$ and $\beta' = 0$ (see Roberge et al. 1991).

REFERENCES.—(1) Estimate; (2) Roberge et al. 1991; (3) Allison & Dalgarno 1970; (4) Cantu et al. 1981; (5) Chapman & Henry 1971, and Dill et al. 1975; (6) Kirby & Goldfield 1991; (7) Stark et al. 1992; (8) Chapman & Henry 1972; (9) Letzelter et al. 1987, and van Dishoeck & Black 1988; (10) Saxon & Liu 1986.

In this expression, f_v are the H_2 absorption line oscillator strengths (Allison & Dalgarno 1970) of the energetically accessible Lyman and Werner band FUV transitions between the ground vibrational of the ground $X^1\Sigma_g$ electronic state and vibrational levels, v , of the excited $B^1\Sigma_u$ and $C^1\Pi_u$ electronic states, η_v are the fractions of FUV absorptions into the levels v that lead to spontaneous radiative dissociations (Stephens & Dalgarno 1972), and $\chi I_\nu(\nu)$ are the incident FUV photon fluxes at the absorption-line transition frequencies. The line self-shielding functions are given by

$$g_v(N_{\text{H}_2}) \equiv \left(\frac{\pi e^2}{mc} f_v \right)^{-1} \frac{dW_v}{dN_{\text{H}_2}} \quad (\text{A4})$$

where W_v are the equivalent widths of the absorption lines, and N_{H_2} is the H_2 column density measured from the cloud surface. We used the analytic formulae of Federman et al. (1979) to compute the self-shielding factors as functions of the H_2 column density. The bi-exponential term in equation (A3) accounts for the decrease in the H_2 photodissociation rate due to FUV continuum grain attenuation. We adopted the H_2 attenuation parameters $\alpha_{\text{H}_2} = 3.78$ and $\beta_{\text{H}_2} = -1.04 \times 10^{-2}$ which we computed (for $A_V^{\text{gr}} = 100$ clouds) assuming optically thin H_2 absorption lines. Equation (A3) yields a H_2 photodissociation rate equal to $4.9 \times 10^{-11} \text{ s}^{-1}$ in a unit Draine field.

Similarly, we used a depth-dependent CO photodissociation rate given by

$$\Gamma_{\text{CO}} = \chi \frac{\pi e^2}{mc} \left[\sum_v I_\nu(\nu) f_v \eta_v \right] \Theta(N_{\text{H}_2}, N_{\text{CO}}) e^{-\alpha_{\text{CO}} A_\nu - \beta_{\text{CO}} A_\nu^2} \text{ s}^{-1}, \quad (\text{A5})$$

where f_v are the FUV absorption line oscillator strengths to predissociating levels in excited electronic states of CO, and η_v are the predissociating fractions (Letzelter et al. 1987; van Dishoeck & Black 1988). CO line shielding occurs due to overlap with broad H_2 absorption lines and opacity in the CO lines themselves. In our model we used the CO shielding function, $\Theta(N_{\text{CO}}, N_{\text{H}_2})$, computed by van Dishoeck & Black (1988) as functions of the H_2 and CO column densities N_{H_2} and N_{CO} . The bi-exponential factor in equation (5) accounts for grain attenuation of the CO photodissociation rate. We set $\alpha_{\text{CO}} = 3.47$ and $\beta_{\text{H}_2} = -1.31 \times 10^{-2}$ which we computed (using the Roberge et al. program) assuming optically thin CO dissociating absorption lines. Equation (A5) yields a CO photodissociation rate equal to $2.0 \times 10^{-10} \text{ s}^{-1}$ in a unit Draine field (van Dishoeck & Black 1988).

A1.2. *Cosmic-Ray-induced Photodestruction*

A flux of FUV photons is maintained in the “dark” cores of molecular clouds by the decay of electronically excited hydrogen molecules produced by H₂ collisions with the energetic secondary electrons generated following the cosmic-ray ionization of H₂ (Prasad & Tarafdar 1983). These photons are absorbed by the dust grains and by atoms and molecules in photoionizations and photodissociations. The rates, R_{cr} , of atomic and molecular photoionization or photodissociation by the cosmic-ray-induced photons may be written as (Gredel et al. 1989)

$$R_{\text{cr}} = \frac{\zeta p}{1 - \omega} \text{ s}^{-1}, \quad (\text{A6})$$

where ζ is the cosmic-ray ionization rate (s⁻¹) of hydrogen, ω is the grain albedo, and p is a factor that depends on the atomic or molecular FUV photoabsorption cross sections. In Table 6 we list the values of p for the cosmic-ray-induced photoreactions that we have included in our calculations. In our model we adopted a grain albedo $\omega = 0.5$.

A1.3. *Chemical Rate Coefficients*

In our calculations we included all of the 772 ion-molecule and neutral-neutral chemical reactions listed in the (UMIST) compilation of Millar et al. (1991) for which the chemical reactants and products are atomic and molecular species included in our model. Only 210 of these reactions significantly influence the cloud chemistry as discussed in § 3 and illustrated in Figures 1–6. We adopted the chemical rate coefficients listed by Millar et al. (1991), except for the dissociative recombinations $\text{H}_3^+ + e \rightarrow \text{H}_2 + \text{H}$ (R26) and $\text{H}_3^+ + e \rightarrow \text{H} + \text{H} + \text{H}$ (R27) for which we adopted rapid rate coefficients equal to $1 \times 10^{-7} (T/300)^{-0.5} \text{ cm}^3 \text{ s}^{-1}$ where T is the gas temperature (K) (Amano 1990; Dalgarno 1993).

A1.4. *H₂ Formation and Excitation*

The H₂ formation rate is a crucial parameter which influences the size and gas temperature of the hot H I zone, and the densities of H₂ and other molecular species in the warm part of the H/H₂ transition layer. In our model we neglected gas-phase H₂ formation

TABLE 6
COSMIC-RAY-INDUCED PHOTODESTRUCTION RATES

Photoreaction	p^a	Reference
OH + $\nu_{\text{cr}} \rightarrow \text{O} + \text{H}$	522	1
H ₂ O + $\nu_{\text{cr}} \rightarrow \text{OH} + \text{H}$	979	1
O ₂ + $\nu_{\text{cr}} \rightarrow \text{O} + \text{O}$	730	1
O ₂ + $\nu_{\text{cr}} \rightarrow \text{O}_2^+ + e$	88	1
C + $\nu_{\text{cr}} \rightarrow \text{C} + e$	510	2
CH + $\nu_{\text{cr}} \rightarrow \text{C} + \text{H}$	756	1
CH ₄ + $\nu_{\text{cr}} \rightarrow \text{CH}_2 + \text{H}_2$	2272	1
S + $\nu_{\text{cr}} \rightarrow \text{S}^+ + e$	1000	4
H ₂ S + $\nu_{\text{cr}} \rightarrow \text{SH} + \text{H}$	5072	1
H ₂ S + $\nu_{\text{cr}} \rightarrow \text{H}_2\text{S}^+ + e$	1555	1
NH ₂ + $\nu_{\text{cr}} \rightarrow \text{NH} + \text{H}$	81	1
NH ₂ + $\nu_{\text{cr}} \rightarrow \text{NH}_2^+ + e$	610	1
NH ₃ + $\nu_{\text{cr}} \rightarrow \text{NH}_2 + \text{H}$	1325	1
NH ₃ + $\nu_{\text{cr}} \rightarrow \text{NH}_2 + \text{H}_2$	541	1
NH ₃ + $\nu_{\text{cr}} \rightarrow \text{NH}_3^+ + e$	543	1
Si + $\nu_{\text{cr}} \rightarrow \text{Si}^+ + e$	1500	3
CO + $\nu_{\text{cr}} \rightarrow \text{C} + \text{O}$	10	2
SO + $\nu_{\text{cr}} \rightarrow \text{S} + \text{O}$	500	4
SO ₂ + $\nu_{\text{cr}} \rightarrow \text{SO} + \text{O}$	1995	1
NO + $\nu_{\text{cr}} \rightarrow \text{N} + \text{O}$	427	1
NO + $\nu_{\text{cr}} \rightarrow \text{NO}^+ + e$	430	1
SiO + $\nu_{\text{cr}} \rightarrow \text{Si} + \text{O}$	1500	3
SiO ₂ + $\nu_{\text{cr}} \rightarrow \text{SiO} + \text{O}$	1500	3
HCN + $\nu_{\text{cr}} \rightarrow \text{CN} + \text{H}$	2986	1
OCS + $\nu_{\text{cr}} \rightarrow \text{CO} + \text{S}$	5371	1
CH ⁺ + $\nu_{\text{cr}} \rightarrow \text{C} + \text{H}^+$	183	1

^a The cosmic-ray-induced photodestruction rates are given in units of the cosmic-ray ionization rate of hydrogen (see text).

REFERENCES.—(1) Gredel et al. 1989; (2) Gredel et al. 1987; (3) Langer & Glassgold 1990; (4) Estimate.

processes and assumed that the hydrogen molecules form on grain surfaces at a rate per unit volume Rn_H (s^{-1}) where n is the total hydrogen particle density, n_H (cm^{-3}) is the atomic hydrogen density, and R is the H_2 -grain formation rate coefficient given by

$$R = 3 \times 10^{-18} f_a S T^{1/2} \text{ cm}^3 \text{ s}^{-1}. \quad (\text{A7})$$

In this expression T is the gas temperature (K), S is the gas-grain sticking coefficient, and f_a is the fraction of hydrogen atoms that do not evaporate from the grain surfaces before molecule formation. The H_2 formation efficiency is uncertain at large gas and grain temperatures (Buch 1989; Buch & Zhang 1991), and in our model we adopted the sticking coefficient given by Burke & Hollenbach (1983)

$$S = [1 + 0.04(T + T_g)^{1/2} + 2 \times 10^{-3}T + 8 \times 10^{-6}T^2]^{-1} \quad (\text{A8})$$

and the fraction

$$f_a = \frac{1}{1 + 10^4 \exp(-600/T_g)} \quad (\text{A9})$$

given by Hollenbach & McKee (1979). The factors S and f_a depend on both the gas temperature and the grain temperature T_g . For $T_g = 30$ K the H_2 formation rate coefficient equals 1.7×10^{-17} and $7.7 \times 10^{-18} \text{ cm}^3 \text{ s}^{-1}$ at a gas temperature of 10^2 and 10^3 K, respectively.

The densities of vibrationally excited hydrogen molecules are important cloud quantities since the internal energies of (suprathermally) excited molecules may be used to drive endothermic hydrogen abstraction reactions of the form



even at low gas temperatures (Jones et al. 1986). For these reactions we adopted rate coefficients

$$k = k_0 \sum_{v=0}^{14} x(v) e^{-(E-E_v)/kT} \text{ cm}^3 \text{ s}^{-1} \quad (\text{A11})$$

where $x(v)$ and E_v are the population fractions and energies of H_2 molecules in vibrational levels v . In this expression E is the reaction endothermicity defined such that for ground state H_2 molecules the rate coefficients are equal to $k_0 \exp(-E/kT)$.

Detailed studies of H_2 excitation in PDRs have been presented elsewhere (Black & Dalgarno 1976; Black & van Dishoeck 1987; Sternberg 1988; Sternberg & Dalgarno 1989; Burton et al. 1990; Goldshmidt & Sternberg 1995). In our calculations we solved the (depth-dependent) equations of statistical equilibrium for the H_2 vibrational level populations, $x(v)$, but we neglected the rotational level distributions within each of the 15 vibrational manifolds. We considered vibrational excitations by FUV-pumping and by collisions with thermal hydrogen atoms and molecules, and vibrational deexcitations by (optically thin) quadrupole radiative transitions and collisions with H and H_2 . We adopted approximate H- H_2 and H_2 - H_2 collisional de-excitation rate coefficients $q_{v \rightarrow v-1} = 5.4 \times 10^{-13} T^{1/2} v$ ($\text{cm}^3 \text{ s}^{-1}$) where T is the gas temperature and v is the vibrational quantum number of the upper level (Sternberg & Dalgarno 1989; Mandy & Martin 1993; Sun & Dalgarno 1994), and upward rate coefficients given by the condition of detailed balance

$$\frac{q_{v-1 \rightarrow v}}{q_{v \rightarrow v-1}} = e^{-(E_v - E_{v-1})/kT}. \quad (\text{A12})$$

We neglected collisions which induce transitions for which $\Delta v > 1$. For these rate coefficients the rates of radiative and collisional deactivation of H_2 molecules in the $v = 1$ level become equal at a critical hydrogen particle density equal to $5 \times 10^4 \text{ cm}^{-3}$ at 10^3 K.

In Table 7 we list the total column densities of vibrationally excited H_2 molecules produced in our model. The total H_2 column density in the $v = 1$ level is large due to the rapid collisional excitation that occurs in the hot part of the H/ H_2 transition layer (see Fig. 8). The excitation of the higher lying vibrational levels is dominated by FUV pumping (Sternberg & Dalgarno 1989).

A2. THERMAL BALANCE

In our model we explicitly computed the equilibrium gas temperatures of the outer cloud layers where the incident FUV radiation field dominates the gas heating. At larger cloud depths, where the gas heating mechanisms are less certain, we adopted a uniform gas temperature equal to 20 K.

The dominant gas heating mechanisms that we included are grain-photoelectric emission (de Jong 1977; Draine 1978), photoionization of "large molecules" (Lepp & Dalgarno 1988; Verstraete et al. 1990), and collisional de-excitation by FUV-pumped H_2 molecules (Sternberg & Dalgarno 1989). We considered gas cooling by atomic and ionic fine-structure line emission, molecular

TABLE 7
VIBRATIONAL H₂ COLUMN
DENSITIES^a

v	N_v (cm ⁻²)
0	1.1 (22)
1	1.6 (17)
2	4.6 (15)
3	1.2 (15)
4	6.8 (14)
5	4.5 (14)
6	3.1 (14)
7	2.2 (14)
8	1.6 (14)
9	1.2 (14)
10	8.6 (13)
11	6.2 (13)
12	4.3 (13)
13	2.8 (13)
14	1.7 (13)

^a Total column densities in each of the 15 vibrational levels of the ground $X^1\Sigma_g^+$ electronic state of H₂ that are produced in a cloud with a total gas density $n_T = 10^6$ cm⁻³ exposed to a FUV field with $\chi = 2 \times 10^5$.

rotational and vibrational line emission, and gas-grain collisions (Tielens & Hollenbach 1985; Sternberg & Dalgarno 1989; Hollenbach & McKee 1989). We describe these processes below.

A2.1. H₂ Heating and Cooling

FUV pumping of the H₂ followed by collisional de-excitation of the vibrational molecular levels heats the gas, and collisional vibrational excitation followed by radiative quadrupole decay cools the gas. The net heating (or cooling) rate due to the collisional energy transfers is

$$G_{H_2} = n_T n(H_2) \sum_v x(v) \sum_{v'} q(v \rightarrow v') (E_v - E_{v'}) \text{ ergs cm}^{-3} \text{ s}^{-1}, \quad (\text{A13})$$

where $n(H_2)$ is the H₂ density, $x(v)$ are the fractions of molecules in each of the vibrational levels v , E_v is the energy of level v , and $q(v \rightarrow v')$ are the collisional rate coefficients for transitions from v to v' . G_{H_2} is positive when the total energy transferred to the gas in collisional deexcitations is greater than the energy lost in collisional excitations.

We have also included gas heating by H₂ photodissociation and molecular formation (Stephens & Dalgarno 1973; Duley & Williams 1986). However, these processes do not contribute significantly to the gas heating (Sternberg & Dalgarno 1989).

A2.2. Photoelectric Emission

Photoelectric emission of electrons from grain surfaces is a major heat source (Watson 1972; Jura 1976; de Jong 1977; Draine 1978; Tielens & Hollenbach 1985; Sternberg & Dalgarno 1989). In our calculations we used Draine's (1978) formalism and grain parameters to compute the photoelectric heating rate which is given by

$$G_{pe} = 4\pi \int_{E_0}^{\epsilon - B_0} (E - eU) dE \int_0^{\epsilon_H} Y(\epsilon) f(E, \epsilon) g(\epsilon) d\epsilon \text{ ergs cm}^{-3} \text{ s}^{-1}, \quad (\text{A14})$$

where B_0 is the photoelectric threshold, $g(\epsilon)$ is the photon radiation intensity for photons with energy ϵ (see eq. [A1]), $Y(\epsilon)$ is the photoelectric yield, E is the energy of the ejected electrons, and $f(E, \epsilon)$ is the energy distribution function for the emitted electrons. The grain potential U is determined by the requirement that in equilibrium the total grain current due to electron and ion recombination onto the grain surfaces and photoelectric emission from the grains vanishes. In our computations we assumed that $B_0 = 8$ eV.

A2.3. PAH Photoionization

Discrete photoionization of large molecules or very small grains may be a major heating mechanism in photon-dominated regions (Lepp & Dalgarno 1988; Wolfire et al. 1995). In our model we assume that large molecules are present in the form of polycyclic aromatic hydrocarbons (PAHs). Such molecules been proposed as the carriers of several broad near-infrared emission features in nebulae (Leger & Puget 1984; d'Hendecourt et al. 1982) although the identifications remain uncertain. We used the data provided by Verstraete et al. (1990) for large planar organic molecules to compute the PAH photoionization rate

$$G_P = \Gamma_P n_P f \left(\langle E \rangle - \frac{2 + \phi}{1 + \phi} kT \right) \text{ ergs cm}^{-3} \text{ s}^{-1}. \quad (\text{A15})$$

as a function of cloud depth. In this expression Γ_P is the photoionization rate of neutral PAHs, $\langle E \rangle$ is the average kinetic energy of the photoelectrons, n_P is the total volume density of PAHs, and

$$f = \frac{k_P n(e)}{\Gamma_P + k_P n(e)} \quad (\text{A16})$$

is the neutral PAH fraction, where $k_P = 1.3 \times 10^{-10} T^{1/2} (1 + \phi)$ is the rate coefficient for recombination of electrons with ionized PAHs, $n(e)$ is the electron density, and $\phi \equiv eU/kT$ where U is the electric potential of the ionized PAHs. Following Verstraete et al. (1990) we set $\langle E \rangle = 2.2 \text{ eV}$, $\phi = 2 \times 10^4 / T$, and $\Gamma_{\text{PAH}} = 2.7 \times 10^{-8} \exp(-2.55 A_V + 1.65 \times 10^{-2} A_V^2)$. In our model we adopted a total PAH abundance $n_P = 10^{-7} n_{\text{H}}$. For this choice the heating rates G_P and G_{PE} are comparable (Lepp & Dalgarno 1988; Verstraete et al. 1990).

A2.4. Fine-Structure Emission

Fine structure line emission from trace atomic and ionic species is a major gas coolant in photon-dominated regions (Dalgarno & McCray 1972; Tielens & Hollenbach 1985; Sternberg & Dalgarno 1989). The cooling rate due to a transition $i \rightarrow j$ of an atom or ion X is

$$L_{ij}^X = n_i A_{ij} h\nu_{ij} \beta(\tau_{ij}) \text{ ergs cm}^{-3} \text{ s}^{-1}, \quad (\text{A17})$$

where n_i is the volume density of the upper fine-structure level i , A is the Einstein coefficient for spontaneous transitions, and ν is the transition frequency. We used an “escape probability” method to compute the cooling in optically thick transitions, and in eq. (A16) $\beta(\tau)$ is the photon escape probability for static plane parallel clouds (de Jong, Chu, & Dalgarno 1975) where τ is the line-center optical depth. We computed the line optical depths assuming Doppler parameters $b = 2 \text{ km s}^{-1}$. In PDRs the atomic and ionic fine-structure levels are excited primarily by neutral impact collisions with hydrogen atoms or molecules. In Table 8 we list the atomic data we used to compute the fine-structure cooling rates. Most of these data were obtained from the compilation of Hollenbach & McKee (1989). In Table 8 we also list the total optical depths and line intensities of the various fine-structure lines that are produced in our model cloud up to a cloud depth $A_V = 10$.

A2.5. Molecular Cooling

Rotational line emission by the trace molecular constituents OH, H₂O, and CO contributes significantly to the gas cooling. OH rotational line cooling is particularly important in the hot part of the H/H₂ transition region, and H₂O and CO line cooling become significant in deeper and cooler cloud layers.

In order to compute the OH and CO cooling rates we used Hollenbach & McKee’s (1979) analytic “universal” molecular cooling function

$$L_{\text{rot}} = \frac{2(kT)^2 A_0 n(X)}{E_0} \left[\frac{2 + y_m + 0.6 y_m^2}{1 + c_\tau + (n_{\text{cr}}/n) + 1.5(n_{\text{cr}}/n)^{1/2}} \right] \text{ ergs cm}^{-3} \text{ s}^{-1}, \quad (\text{A18})$$

where

$$y_m = \ln \left[1 + \frac{c_\tau}{1 + 10(n_{\text{cr}}/n)} \right], \quad (\text{A19})$$

$n(X)$ is the molecular density, A_0 and E_0 are the radiative transition probability and energy of the lowest rotational transition, n_{cr} is the critical density for the level whose energy equals kT , and c_τ is a line optical depth factor. We used the CO and OH cooling parameters recommended by Hollenbach & McKee (1979). Detailed treatments of CO line emission from PDRs have been presented by Burton et al. (1990), Köster et al. (1994), and Wolfire et al. (1993).

TABLE 8
FINE-STRUCTURE COOLING DATA^a

Species	<i>j</i>	<i>i</i>	<i>E</i> ^b (K)	λ (μm)	<i>A</i> (s ⁻¹)	α^c	β	Column Partner	<i>I</i> ^d (cgs)	τ^e	Reference
C ⁺	² P _{1/2}	² P _{3/2}	92	157.7	2.4 (-6)	5.8 (-10)	0.02	H	1
						3.1 (-10)	0.1	H ₂	1.26 (-3)	6.5 (-1)	2
Si ⁺	² P _{1/2}	² P _{3/2}	414	34.8	2.1 (-4)	6.5 (-10)	0.0	H, H ₂	1.13 (-3)	2.8 (-2)	3
C	³ P ₀	³ P ₁	24	609.2	7.9 (-8)	1.3 (-10)	0.045	H, H ₂	8.2 (-7)	2.2 (-1)	4
	³ P ₁	³ P ₂	39	369.0	2.7 (-7)	7.8 (-11)	0.035	H, H ₂	2.9 (-6)	1.3 (-1)	4
	³ P ₀	³ P ₂	63	229.9	2.0 (-14)	2.0 (-10)	0.084	H, H ₂	3.6 (-13)	7.2 (-9)	4
O	³ P ₂	³ P ₁	228	63.2	9.0 (-5)	4.2 (-12)	0.67	H	4
						2.3 (-11)	0.38	H ₂	6.9 (-2)	1.6 (1)	5
	³ P ₁	³ P ₀	98	145.6	1.7 (-5)	1.5 (-11)	0.4	H	4
						4.4 (-11)	0.35	H ₂	2.1 (-3)	2.0 (-1)	5
	³ P ₂	³ P ₀	326	44.2	1.0 (-10)	1.1 (-12)	0.44	H	4
						1.7 (-12)	0.12	H ₂	4.2 (-8)	2.1 (-6)	5
S	³ P ₂	³ P ₁	571	25.2	1.4 (-3)	7.5 (-10)	...	H, H ₂	1.3 (-5)	2.2 (-1)	3
	³ P ₁	³ P ₀	255	56.6	3.0 (-4)	4.2 (-10)	...	H, H ₂	3.5 (-7)	5.3 (-12)	3
	³ P ₂	³ P ₀	826	17.4	7.1 (-8)	7.1 (-10)	...	H, H ₂	1.8 (-16)	1.2 (-12)	3
Fe ⁺	⁶ D _{9/2}	⁶ D _{7/2}	554	26.0	2.5 (-3)	9.5 (-10)	...	H, H ₂	3.1 (-3)	1.2 (-1)	6
	⁶ D _{7/2}	⁶ D _{5/2}	407	35.4	1.6 (-3)	4.7 (-10)	...	H, H ₂	6.9 (-4)	1.2 (-3)	6
	⁶ D _{9/2}	⁶ D _{5/2}	961	15.0	1.5 (-9)	5.7 (-10)	...	H, H ₂	1.5 (-9)	1.2 (-8)	6

^a Most of the fine-structure data listed in this table were taken from the compilation presented by Hollenbach & McKee 1989. Individual references for the collisional rate coefficients are given below.

^b Upper level energies above ground.

^c Collisional de-excitation rate coefficients for collisions with atomic or molecular hydrogen are $qH = \alpha T^\beta \text{ cm}^3 \text{ s}^{-1}$. A_{ij} is the radiative transition probability between levels *i* and *j*.

^d The total fine-structure line intensities produced (within a cloud depth $A_\nu = 10$) in our model calculation are given as (cgs) units of $\text{ergs s}^{-1} \text{ cm}^{-2} \text{ sr}^{-1}$.

^e τ is the fine-structure line-center optical depth (at $A_\nu = 10$).

REFERENCES.—(1) Launay & Roueff 1977a; (2) Flower & Launay 1977; (3) Hollenbach & McKee 1989; (4) Launay & Roueff 1977b; (5) Jaquet et al. 1992; (6) Aannestad 1973.

For the polyatomic molecule H₂O we used the expression provided by Neufeld & Melnick (1987)

$$L_{\text{H}_2\text{O}} = \frac{3.67 \times 10^{-29} T^{1.95} n_{\text{H}} n(\text{H}_2\text{O})}{1 + \sqrt{n_{\text{H}} N_{\text{H}_2\text{O}} / (1.4 \times 10^{11} b T^{2.9})}} \text{ ergs cm}^{-3} \text{ s}^{-1} \quad (\text{A20})$$

for the total water line emissivity in static clouds. In this expression $n(\text{H}_2\text{O})$ and $N_{\text{H}_2\text{O}}$ are the volume and column water densities, and $b = 2 \text{ km s}^{-1}$ is the emission line Doppler parameter. In Table 9 we list the total OH, H₂O, and CO rotational emission intensities produced in our model cloud.

A3. NUMERICAL METHOD

Equations (1)–(4) (in §§ 2 and 3) are a set of nonlinear coupled ordinary differential equations for the atomic and molecular column densities $N_i(z)$. We used the Newton-Raphson method to solve the set of nonlinear (algebraic) equations (1), (2), and (3), and we employed the Bulirsch-Stoer adaptive step-size extrapolation algorithm (Press et al. 1986) to compute the atomic and molecular column densities.

TABLE 9
MOLECULAR COOLING EMISSION^a

Molecule	<i>I</i> (cgs)
OH	5.9 (-3)
H ₂ O	1.4 (-4)
CO	6.7 (-3)

^a Total molecular rotational emission line intensities ($\text{ergs s}^{-1} \text{ cm}^{-1} \text{ sr}^{-1}$) produced in a cloud with $n_T = 10^6 \text{ cm}^{-3}$ exposed to a FUV radiation field with $\chi = 2 \times 10^5$.

REFERENCES

- Aannestad, P. 1973, *ApJS*, 25, 223
- Abgrall, H., Le Bourlot, J., Pineau des Forets, G., Roueff, E., Flower, D. R., & Heck, L. 1992, *A&A*, 265, 403
- Allison, A. C., & Dalgarno, A. 1970, *Atomic Data Tables*, 1, 289
- Amano, T. 1990, *J. Chem. Phys.*, 96, 6492
- Black, J. H., & Dalgarno, A. 1976, *ApJ*, 203, 132
- Black, J. H., & van Dishoeck, E. F. 1987, *ApJ*, 322, 412
- Blietz, M., Cameron, M., Drapatz, S., Genzel, R., Krabbe, A., van der Werf, P. V. D., Sternberg, A., & Ward, M. 1994, *ApJ*, 412, 92
- Breukers, R. 1991, Ph.D. thesis, Univ. of Leiden
- Buch, V. 1989, in *Evolution of Interstellar Dust and Related Topics*, ed. A. Bonetti, J. M. Greenberg, & S. Aiello (Società Italiana di Fisica) (Amsterdam: North-Holland), 321
- Buch, V., & Zhang, Q. 1991, *ApJ*, 379, 647
- Burton, M., Hollenbach, D., & Tielens, A. G. G. M. 1990, *ApJ*, 365, 620
- Burke, J. R., & Hollenbach, D. J. 1983, *ApJ*, 265, 223
- Cantu, A. M., Mazzoni, M., Pettini, M., & Tozzi, G. P. 1981, *Phys. Rev. A*, 23, 1223
- Chapman, R. D., & Henry, R. J. W. 1971, *ApJ*, 168, 169
- . 1972, *ApJ*, 173, 243
- Dalgarno, A., & Black, J. H. 1976, *Rep. Prog. Phys.*, 39, 573
- Dalgarno, A., & McCray, R. A. 1972, *ARA&A*, 10, 375
- Dalgarno, A. 1993, in *Adv. Atom. Molec. Opt. Phys.*, 32, 57
- de Jong, T. 1977, *A&A*, 55, 137
- de Jong, T., Chu, S. I., & Dalgarno, A. 1975, *ApJ*, 199, 69
- de Jong, T., Dalgarno, A., & Boland, A. 1980, *A&A*, 91, 68
- d'Hendecourt, L. B., Allamandola, L. J., Baas, F., & Greenberg, J. M. 1982, *A&A*, 109, L12
- Dill, D., Starace, A. F., & Manson, S. T. 1975, *Phys. Rev. A*, 11, 1596
- Draine, B. T. 1978, *ApJS*, 36, 595
- Draine, B. T., & Lee, H. M. 1984, *ApJ*, 285, 89
- Duley, W. W., & Williams, D. A. 1986, *MNRAS*, 223, 177
- Elmegreen, B. G. 1993, *ApJ*, 411, 170
- Encrenaz, Th., & Kessler, M. F. 1992, *Infrared Astronomy with ISO* (New York: Nova Science Publishers)
- Federman, S. R., Glassgold, A. E., & Kwan, J. 1979, *ApJ*, 227, 446
- Flower, D. R., & Launay, J. M. 1977, *J. Phys. B*, 10, 3673
- Fuente, A., Martin-Pintado, J., Cernicharo, J., & Bachillerio, R. 1993, *A&A*, 276, 473
- Genzel, R. 1992, in *The Galactic Interstellar Medium: Saas Fe Lectures 1991* (New York: Springer)
- Genzel, R., Harris, A. I., & Stutzki, J. 1989, in *Infrared Spectroscopy in Astronomy*, ed. B. H. Kaldeich, ESA-SP 290, 115
- Genzel, R., Hollenbach, D. H., & Townes, C. H. 1994, *Phys. Rep.*, in press
- Goldshmidt, O., & Sternberg, A. 1995, *ApJ*, 439, 256
- Graham, J. R., Serabyn, E., Herbst, T. M., Matthews, K., Neugebauer, G., Soifer, B. T., Wilson, T. D., & Beckwith, S. 1993, *ApJ*, 408, L105
- Gredel, R., Lepp, S., & Dalgarno, A. 1987, *ApJ*, 323, L137
- Gredel, R., Lepp, S., Dalgarno, A., & Herbst, E. 1989, *ApJ*, 347, 289
- Harris, A. I., Jaffe, D. T., Stutzki, J., & Genzel, R. 1987, *Internat. J. IR MM Waves*, 8, 857
- Henkel, C., Baan, W. A., & Mauersberger, R. 1991, *A&A Rev.*, 3, 47
- Hogerheijde, M. R., Jansen, D. J., & van Dishoeck, E. F. 1995, *A&A*, 294, 792
- Hollenbach, D. J. 1990, in *The Evolution of the Interstellar Medium*, ed. L. Blitz (San Francisco: ASP), 167
- Hollenbach, D., & McKee, C. F. 1979, *ApJS*, 41, 555
- . 1989, *ApJ*, 342, 306
- Hollenbach, D. J., Takahashi, T., & Tielens, A. G. G. M. 1991, *ApJ*, 377, 192
- Howe, J. E., Jaffe, D. T., Genzel, R., & Stacey, G. J. 1991, *ApJ*, 373, 158
- Jackson, J. M., Paglione, T. A. D., Ishizuki, S., & Rieu, N. Q. 1993, *ApJ*, 418, L13
- Jaffe, D. T., & Howe, J. E. 1989, *Rev. Mexicana Astron. Af.*, 18, 55
- Jansen, D. J., van Dishoeck, E. F., & Black, J. H. 1994, *A&A*, 282, 605
- Jaquet, R., Staemmler, V., Smith, M. D., & Flower, D. R. 1992, *J. Phys. B*, 25, 285
- Jones, E., Barlow, S. E., Ellison, G. B., & Ferguson, E. E. 1986, *Chem. Phys. Lett.*, 130, 218
- Jura, M. 1976, *ApJ*, 204, 12
- Kirby, K. P., & Goldfield, E. M. 1991, *J. Chem. Phys.*, 94, 1271
- Köster, B., Störzer, H., Stutzki, J., & Sternberg, A. 1994, *A&A*, in press
- Krabbe, A., et al. 1993, *PASP*, 105, 694
- Krabbe, A., Sternberg, A., & Genzel, R. 1994, *ApJ*, 425, 72
- Lane, A. P., Haas, M. R., Hollenbach, D. J., & Erickson, E. F. 1990, *ApJ*, 361, 132
- Langer, W. D., & Glassgold, A. E. 1990, *ApJ*, 352, 123
- Latter, W. B., Walker, C. K., & Maloney, P. R. 1993, *ApJ*, 419, L97
- Launay, J. M., & Roueff, E. 1977a, *A&A*, 56, 289
- . 1977b, *J. Phys. B*, 10, 879
- Le Bourlot, J., Pineau des Forets, G., Roueff, E., & Flower, D. R. 1993, *A&A*, 267, 233
- Leger, A., & Puget, J. L. 1984, *A&A*, 137, L5
- Lepp, S., & Dalgarno, A. 1988, *ApJ*, 335, 769
- Letzelter, C., Eidelsberg, M., Rostas, F., Breton, J., & Thieblemont, B. 1987, *J. Chem. Phys.*, 114, 274
- Mandy, M. E., & Martin, P. G. 1993, *ApJS*, 86, 199
- Mathis, J. S., Ruml, W., & Nordsieck, K. H. 1977, *ApJ*, 217, 425
- McKee, C. F. 1989, *ApJ*, 345, 782
- Meixner, M., Haas, M. R., Tielens, A. G. G. M., Erickson, E. F., & Werner, M. 1992, *ApJ*, 390, 499
- Meixner, M., & Tielens, A. G. G. M. 1993, *ApJ*, 405, 216
- Millar, T. J., Rawlings, J. M. C., Bennet, A., Brown, P. D., & Charnley, S. B. 1991, *A&AS*, 87, 585
- Neufeld, D. A., & Dalgarno, A. 1989, *ApJ*, 340, 869
- Neufeld, D. A., & Melnick, G. J. 1987, *ApJ*, 322, 266
- Phillips, T. G. 1992, in *Astronomy with Millimeter and Submillimeter Wave Interferometry*, IAU Symp. 140, ed. M. Ishiguro (Dordrecht: Reidel), 68
- Planesas, P., Scoville, N., & Myers, S. T. 1991, *ApJ*, 369, 364
- Poglitsch, A., et al. 1991, *Internat. J. IP MM Waves*, 12, 859
- Prasad, S. S., & Huntress, W. T. 1979, *ApJS*, 43, 1
- Prasad, S. S., & Tarafdar, S. P. 1983, *ApJ*, 267, 603
- Press, W. H., Flannery, B. P., Teukolsky, S. A., & Vetterling, W. T. 1986, in *Numerical Recipes* (Cambridge: Cambridge Univ. Press), 563
- Roberge, W. G., Jones, D., Lepp, S., & Dalgarno, A. 1991, *ApJS*, 77, 287
- Rotaciuc, V., Krabbe, A., Cameron, M., Drapatz, S., Genzel, R., Sternberg, A., & Storey, J. W. V. 1991, *ApJ*, 370, L23
- Sargent, A. I., & Welch, W. J. 1993, *ARA&A*, 31, 297
- Saxon, R. P., & Liu, B. 1986, *J. Chem. Phys.*, 85, 2099
- Shalabiea, O. M., & Greenberg, J. M. 1994, *A&A*, 290, 266
- Shu, F. H., Adams, F. C., & Lizano, S. 1987, *ARA&A*, 25, 23
- Stacey, G. J., Geis, N., Genzel, R., Lugten, J. B., Poglitsch, A., Sternberg, A., & Townes, C. H. 1991, *ApJ*, 373, 423
- Stacey, G. J., Jaffe, D. T., Geis, N., Genzel, R., Harris, A. I., Poglitsch, A., Stutzki, J., & Townes, C. H. 1993, *ApJ*, 404, 219
- Stark, G., Smith, P. L., Huber, K. P., Yoshino, K., Stevens, M. H., & Ito, K. 1992, *J. Chem. Phys.*, 97, 4809
- Stephens, T. L., & Dalgarno, A. 1972, *J. Quant. Spectrosc. Rad. Tran.*, 12, 569
- . 1973, *ApJ*, 186, 165
- Sternberg, A. 1988, *ApJ*, 332, 400
- Sternberg, A., Blietz, M., Cameron, M., Genzel, R., Krabbe, A., & Tacconi, L. J. 1994, in *Violent Star Formation: From 30 Doradus to QSOs*, ed. G. Tenorio-Tagle (Cambridge: Cambridge Univ. Press), 263
- Sternberg, A., & Dalgarno, A. 1989, *ApJ*, 338, 197
- Sternberg, A., Dalgarno, A., & Lepp, S. 1987, *ApJ*, 320, 676
- Störzer, H., Stutzki, J., & Sternberg, A. 1995, *A&A*, 296, L9
- Stutzki, J., Stacey, G. J., Genzel, R., Harris, A. I., Jaffe, D. T., & Lugten, J. B. 1988, *ApJ*, 332, 379
- Sun, Y., & Dalgarno, A. 1994, *ApJ*, 427, 1053
- Tacconi, L. J., Genzel, R., Blietz, M., Cameron, M., Harris, A. I., & Madden, S. 1994, *ApJ*, 426, L77
- Tielens, A. G. G. M., & Hollenbach, D. 1985, *ApJ*, 291, 722
- Tielens, A. G. G. M., et al. 1993, *Science*, 262, 86
- van der Werf, P. P., Goss, W. M., Heiles, C., Crutcher, R. M., & Troland, T. H. 1993, *ApJ*, 411, 247
- van der Werf, P. P., Stutzki, J., Sternberg, A., & Krabbe, A. 1995, *A&A*, submitted

- van Dishoeck, E. F. 1988, in *Millimetre and Submillimetre Astronomy*, ed. W. B. Burton & R. D. Wolstencroft (Dordrecht: Kluwer), 117
- van Dishoeck, E. F., & Black, J. H. 1986, *ApJS*, 62, 109
- . 1988, *ApJ*, 334, 771
- . 1989, *ApJ*, 340, 273
- Verstraete, L., Leger, A., d'Hendecourt, L., Dutuit, O., & Defourneau, D. 1990, *A&A*, 237, 436
- Watson, W. D. 1972, *ApJ*, 176, 103
- Wolfire, M. G., Hollenbach, D., McKee, C. F., Tielens, A. G. G. M., & Bakes, E. L. O. 1995, *ApJ*, 443, 152
- Wolfire, M. G., Hollenbach, D. J., & Tielens, A. G. G. M. 1993, *ApJ*, 402, 195
- Wolfire, M. G., Tielens, A. G. G. M., & Hollenbach, D. J. 1990, *ApJ*, 358, 116
- Zhou, S., Evans, N. J., II, Mundy, L., & Kutner, M. L. 1991, *ApJ*, 372, 518
- Zhou, S., Jaffe, D. T., Howe, J. E., Geis, N., Herrmann, F., Madden, S. C., Poglitsch, A., & Stacey, G. J. 1993, *ApJ*, 419, 190